International Journal of Biological Macromolecules 153 (2020) 779–795

Contents lists available at ScienceDirect

International Journal of Biological Macromolecules

journal homepage: http://www.elsevier.com/locate/ijbiomac

# Fibrinogen-clotting enzyme, pictobin, from *Bothrops pictus* snake venom. Structural and functional characterization

Dan E. Vivas-Ruiz [a,*,1], Gustavo A. Sandoval [a,1], Edgar Gonzalez-Kozlova [b], Jacquelyne Zarria-Romero [c], Fanny Lazo [a,1], Edith Rodríguez [a,1], Henrique P.B. Magalhães [d], Carlos Chávez-Olortegui [e], Luciana S. Oliveira [f], Valeria G. Alvarenga [f], Félix A. Urra [g,1], Jorge Toledo [h,i], Armando Yarlequé [a,1], Johannes A. Eble [j], Eladio F. Sanchez [f,1]

[a] Laboratorio de Biología Molecular, Facultad de Ciencias Biológicas, Universidad Nacional Mayor de San Marcos, Lima, Perú, Av. Venezuela Cdra 34 S/N, Ciudad Universitaria, Lima 01, Lima, Peru
[b] Department of Genetics and Genomic Sciences, Icahn School for Data Science and Genomic Technology, New York, NYC, USA
[c] Laboratorio de Reproducción y Biología del Desarrollo, Facultad de Ciencias Biológicas, Universidad Nacional Mayor de San Marcos, Lima, Perú, Av. Venezuela ra 34 S/N, Ciudad Universitaria, Lima 01, Lima, Peru
[d] Departamento de Análises Clínicas e Toxicológicas, Faculdade de Farmácia, Universidade Federal de Minas Gerais, Belo Horizonte 31270-901, Minas Gerais, Brazil
[e] Departamento de Bioquímica-Inmunología, Instituto de Ciências Biologicas, Universidade Federal de Minas Gerais, Belo Horizonte 31270-901, Minas Gerais, Brazil
[f] Research and Development Center, Ezequiel Dias Foundation, 30510-010 Belo Horizonte, MG, Brazil
[g] Programa de Farmacología Clínica y Molecular, Instituto de Ciencias Biomédicas (ICBM), Facultad de Medicina, Universidad de Chile, Independencia 1027, Casilla 7, Santiago 7800003, Chile
[h] Instituto de Neurociencia Biomédica, Facultad de Medicina, Universidad de Chile, Independencia 1027, Santiago 8380453, Chile
[i] Facultad de Ciencias de la Salud, Universidad San Sebastián, Lota 2465, Providencia, Santiago 7510157, Chile
[j] Institute for Physiological Chemistry and Pathobiochemistry, University of Münster, 48149 Münster, Germany

ARTICLE INFO

*Article history:*
Received 12 November 2019
Received in revised form 9 March 2020
Accepted 9 March 2020
Available online 10 March 2020

*Keywords:*
*Bothrops pictus*
Thrombin-like enzyme
Snake venom
Mitochondrial bioenergetics
Oxidative phosphorylation
Cancer cells

ABSTRACT

A thrombin-like enzyme, pictobin, was purified from *Bothrops pictus* snake venom. It is a 41-kDa monomeric glycoprotein as showed by mass spectrometry and contains approx. 45% carbohydrate by mass which could be removed with N-glycosidase. Pictobin coagulates plasma and fibrinogen, releasing fibrinopeptide A and induces the formation of a friable/porous fibrin network as visualized by SEM. The enzyme promoted platelet aggregation in human PRP and defibrination in mouse model and showed catalytic activity on chromogenic substrates S-2266, S-2366, S-2160 and S-2238. Pictobin interacts with the plasma inhibitor α2-macroglobulin, which blocks its interaction with fibrinogen but not with the small substrate BApNA. Heparin does not affect its enzymatic activity. Pictobin cross reacted with polyvalent bothropic antivenom, and its deglycosylated form reduced its catalytic action and antivenom reaction. In breast and lung cancer cells, pictobin inhibits the fibronectin-stimulated migration. Moreover, it produces strong NADH oxidation, mitochondrial depolarization, ATP decrease and fragmentation of mitochondrial network. These results suggest by first time that a snake venom serinprotease produces mitochondrial dysfunction by affecting mitochondrial dynamics and bioenergetics. Structural model of pictobin reveals a conserved chymotrypsin fold β/β hydrolase. These data indicate that pictobin has therapeutic potential in the treatment of cardiovascular disorders and metastatic disease.



## 1. Introduction

Snake venoms, particularly those of the Viperidae family (pit vipers and true vipers) contain high levels of serine proteinases (SVSPs) and metalloproteinases (SVMPs) among other toxins, which disrupt normal physiological processes such as coagulation and hemostasis. They may cause consumption of clotting factors and hypofibrinogenemia in human victims or experimental animals [1,2]. A group of SVSPs known as fibrinogen-clotting (thrombin-like enzymes, SV-TLEs) have been investigated by their potential therapeutic application (defibrination), as diagnostic reagents and as appropriate models to study mechanism of coagulation *in vitro* [3,4]. SVSPs are widely distributed among

*Abbreviations:* SV-TLE, snake venom thrombin-like enzyme; Fg, fibrinogen; FpA, fibrinopeptide A; FpB, fibrinopeptide B; DL-BAPNA, α-N-benzoyl-DL-arginine-*p*-nitroanilide; *p*NA, *p*-nitroanilide; EDTA, ethylene diamine tetraacetic acid; SBTI, soybean trypsin inhibitor; PMSF, phenyl methyl sulfonyl fluoride; MDD, minimum defibrinogenating dose; TLCK, N-tosyl-lysine chloromethyl ketone; TPCK, tosyl phenylalanyl chloromethyl ketone; DTT, dithiothreitol; 2β-ME, 2β-mercaptoethanol; SEM, scanning electron microscopy; OXPHOS, oxidative phosphorylation; FCCP, carbonyl cyanide-4-(trifluoromethoxy) phenylhydrazone; Olig, oligomycin; NADH, Nicotinamide adenine dinucleotide (reduced); ROS, reactive oxygen species.

* Corresponding author at: Laboratorio de Biología Molecular-Facultad de Ciencias Biológicas, Universidad Nacional Mayor de San Marcos, Cdra 34 S/N, Ciudad Universitaria, Lima 01, Lima, Peru.
*E-mail address:* dvivasr@unmsm.edu.pe (D.E. Vivas-Ruiz).
[1] Network for snake venom research and drug discovery.

https://doi.org/10.1016/j.ijbiomac.2020.03.055
0141-8130/

the Viperid venoms and especially abundant in *Bothrops* venoms [5]. They belong to the trypsin S1A family of PA(S) clan, which are synthesized as zymogens (~260 aa) [4–6]. In spite of 57–85% amino acid sequence identity among SVSPs, they are quite specific toward a given macromolecular substrate [6]. In general, they are single-chain glycoproteins showing typical chymotrypsin-like fold with the catalytic site cleft residing between two β-barrels, with the exception of their additional sixth disulfide linkage and C-terminal extension, which are unique features conserved in venom serine peptidases [7]. Importantly, most SVSPs are glycoproteins, bearing a variable number of N-linked glycosylation sites in non-homologous positions in their sequence, resulting in comparatively high molecular masses of even up to 67-kDa. The function of carbohydrate moieties was revealed for some of these enzymes. Among these functions, the carbohydrate content plays an important role in the interaction with substrates and consequently to maintain and/or improve their catalytic activity [3,6]. These enzymes display quite diverse substrate specificity, causing their versatility in pharmacological action on hemostatic system [3,6–10]. Thus, SVSPs are classified according to their activity into nine basic group: prothrombin activators, Factor X, VII, or V activators, plasminogen activators, serine proteinase inhibitors (serpins), platelet aggregation inducers, fibrin(ogen)olytic enzymes and thrombin-like enzymes (SV-TLEs) [2,4].

Most of coagulant SV-TLEs cause clotting of fibrinogen (Fg). Their molecular mechanism is partially similar to the one thrombin. Depending on the rates and cleavage specificity, with which they cleave off the fibrinopeptide from Fg, either A (FpA) or B (FpB), or both of them, these enzymes are classified into three groups termed venombin A, B or AB [2]. Furthermore, they have significant sequence similarities with thrombin, but SV-TLEs differ considerably in several functional properties such as: 1) a distinct preference to release FPA or FPB or both, 2) the absence of allosteric modulators, 3) the insensitivity to thrombin inhibitors (antithrombin III, hirudin and heparin) for most of them, and 4) they generally do not activate another coagulation factor, but some of them may induce platelet aggregation [5–8]. Insights into the mechanism of action of serine proteinases showed that they employ a catalytic triad of serine (Ser195), histidine (His57) and aspartate (Asp102), with the residue numbering according to the α-chymotrypsinogen system [9], which is absolutely conserved among mammalian serine proteinases [8–10]. The anticoagulant action of SV-TLEs may occur in two forms: (i) by pseudo-procoagulant effect in which part of the coagulation cascade is catalyzed to produce unstable and poorly cross-linked clots, which are readily torn off from the site of formation, at even low shear forces, and (ii) by true anticoagulant effects where clot formation is directly impeded [11,12]. As a consequence of these differences, endogenous Fg decreases considerable and turns the blood uncoagulable. This hemostasis-blocking effect together with vessels wall degradation by venom proteinases lead to detrimental bleeding. Among the latter are metalloproteinases, which hydrolyze key components of the subendothelial basement membrane resulting in severe hemorrhage in the snakebite victim [2,9,10]. This persistent conversion of fibrinogen into fibrin and dissolution of friable and translucent thrombi results in consumptive coagulopathy and eventually leads to the inability to form stable thrombus. Other effects reported for SV-TLEs include activation of the complement system [13,14], alteration of the nervous and muscle systems [15,16].

The pit viper *Bothrops pictus* (Tschudi, 1845; Desert lancehead, Jergón de la costa) is one of the medically most important venomous snake in Peru. This species occurs on arid to semiarid costal foothills, river valleys and dry lower Andean slopes of the western Andes of Peru, from the central to northern Pacific coast between the Departments of Arequipa and the south of the Department of Ancash [17]. Due to its propensity to living near human settlements, it could be found in some of the arid valleys and low mountains close to Lima city. Thus, from January 1990 to April 1998, 23 cases of bothropic accidents were reported in the northern districts (Cono Norte) of the metropolitan area of Lima and assigned to *B. pictus* envenoming as the unique causative agent at the National Hospital Cayetano Heredia (Lima) [18]. Furthermore, from 2014 to date 100 cases of snakebites were registered in the Department of Lima, according to Centro Nacional de Epidemiología, Prevención y Control de Enfermedades – MINSA. Notably, due to rapid access to health services all patients received adequate treatment with anti-bothropic serum (Instituto Nacional de Salud, INS) within the first six hours. This data also supports the efficacy of the antivenom, raised at INS to neutralize the main toxic effects of *Bothrops* venoms.

Although *B. pictus* is medically highly relevant due to its geographical distribution, the pathophysiological mechanism of envenomation caused by *B. pictus*, is poorly understood as the venom compositions of this snake has been rarely investigated from the perspective of potential lead compound development [19,20]. In a preliminary study [21] we reported the purification of pictobin, a fibrinogen-clotting enzyme from *B. pictus* venom called pictobin (Mr = 52 kDa). Sequence analysis revealed that it is a SV-TLE. The present work aimed to characterize the structural and functional profile of pictobin in detail. Unprecedently, we demonstrate that a snake venom serine proteinase produces mitochondrial dysfunction by affecting mitochondrial dynamics and bioenergetics in culture cells. Taken together, this report highlights that glycosylated proteinases that target Fg and produced defibrinogenation *in vivo*, underlines the re-emerging interest in SVSPs as potential therapeutic leads in the development of novel anti-thrombotic and anti-cancer agent.

## 2. Materials and methods

### 2.1. Venom, antivenoms and reagents

*Bothrops pictus* venom was collected from four adults specimens (3 males and 1 female) captured within the district of Pachacamac (southern of Lima, Perú), and kept in captivity at the Serpentarium "Oswaldo Meneses" - Museo de Historia Natural, Universidad Nacional Mayor de San Marcos (UNMSM), Lima, Perú. CM-Sephadex C-50, Sephadex G-100 and G-75, bovine thrombin, PNGase F, and *o*-glycosidase, human fibrinogen essentially plasminogen free, fibrinopeptides A and B, DL-BApNA, trypsin, α2-macroglobulin of human origin and factor XIII, antimycin A, FCCP and oligomycin were obtained from Sigma Chemical Co. p-nitroanilide substrates: D-Phe-Pip-Arg-pNA (for thrombin, S-2238), D-Val-Leu-Lys-pNa (for plasmin, S-2251), D-Pro-Leu-Arg-pNa (for aPC and XIa, S-2366) and D-Val-Leu-Arg-pNa (S-2266) were from Chromogenix. Other substrates D-Phe-Val-Arg-pNA (for thrombin) and Bz-Pro-Leu-Arg-pNA (for plasma kallikrein) were synthesized at the Federal University of São Paulo, Escola Paulista de Medicina (UNIFESP), Saõ Paulo, Brazil. Peruvian antibotropic polyvalent antiserum (αBS-INS, Batch: 01000269) was obtained from Instituto Nacional de Salud (INS) Lima-Perú and Brazilian antibotropic antiserum (αBS-FUNED, Batch 05101833) from Fundação Ezequiel Dias (FUNED), Belo Horizonte-Brazil. All other chemicals were of analytical grade.

For *in vivo* assays, males Balb c mice (18–22 g) were acquired from the bioterium of the INS. All *in vivo* experiments were in accordance with ethical recommendations of the International Guiding Principles for Biomedical Research Involving Animals of the Council of International Organizations of Medical Sciences (CIOMS).

### 2.2. Pictobin purification

Lyophilized *B. pictus* venom (~220 mg) was dissolved in 1 mL of ammonium acetate buffer (0.05 M, pH 6.0), homogenized until complete dissolution and centrifuged (4000 *g* for 20 min). The supernatant (200 mg protein) was applied onto CM-Sephadex C-50 (1.2 × 47.5 cm) column, equilibrated in the above buffer and eluted with a linear salt gradient of 0.1–1 M NaCl at flow rate of 14 mL/h. Fractions containing amidolytic activity were collected and concentrated to

1.2 mL using Ultracell Centrifugal Filter Unit (Amicon). This material (33.9 mg) was further purified through a Sephadex G-100 column (1.4 × 64 cm), equilibrated and eluted with the same buffer at 13 mL/h. Active fractions containing amidolytic activity were concentrated (5.4 mg). This material was applied on a Sephadex G-75 column (1.0 × 30 cm), equilibrated and eluted with the same buffer at 14 mL/h. The homogeneity of pictobin was evidenced by RP-HPLC using a Vydac C18 (4.6 × 250 mm) column, previously equilibrated with 0.1% trifluoroacetic acid (TFA) in water (solution A). The protein was eluted using linear gradient from solution A to 100% 0.1% TFA in acetonitrile (solution B) for 70 min at a flow rate of 1 mL/min. The elution was monitored by absorbance at 280 nm and analyzed by SDS-PAGE according to Laemmli [22].

### 2.3. Molecular mass determination by MALDI-TOF

Protein masses were determined by Matrix-Assisted Laser Desorption Ionization Time of Flight (MALDI-TOF) mass spectrometry as described [23]. Spectra were recorded and analyzed using a Bruker Autoflex III Smartbean instrument in a linear positive mode controlled by the proprietary COMPASS™ 1.2.

### 2.4. Deglycosylation of pictobin

50 μg of pictobin was dissolved in 50 μL of denaturing buffer (0.5% SDS, 1% 2β-ME). The solution was denatured by boiling for 5 min. After addition of 50 μL of reaction buffer (50 mM Tris HCl, pH 8.0), 2.5 μL of detergent solution (IGEPAL 15%, Roche) and 2 units of recombinant PNGase F or *O*-glycosidase, the samples were incubated for 24 h at 37 °C as described elsewhere [24]. The native and deglycosylated proteins were analyzed by reduced SDS-PAGE. In order to maintain its activity, pictobin was also deglycosylated under non denaturing conditions as reported [24,25].

### 2.5. Gene expression analysis of pictobin

RNA (10 ng) was obtained from fresh venom as according to [25]. The level of pictobin expression was performed with real time PCR using Verso 1-Step qPCR ROX Kit (Thermo Fisher Scientific). The master mix was prepared following the manufacturer's instructions. The assay was carried out in a 7500 Applied Biosystem Thermocycler. The phospholipase $A_2$ and L-amino acid oxidase genes were used for comparison and GAPDH as housekeeping gene, was taken as standard.

### 2.6. Pictobin biochemical characterization

#### 2.6.1. Enzyme assays and inhibition studies

Amidolytic activity was determined using DL-BApNA as substrate according to [26]. Clotting activity was measured by mixing appropriate concentrations of pictobin (0.5–2.4 μg) with 0.98 mL of bovine or human Fg (3.5 mg/mL) in 100 mM Tris-HCl buffer, pH 7.4, containing 1 mM $CaCl_2$ at 37 °C. Additionally, the minimum coagulant dose (MCD) was measured *in vitro* using either bovine or human Fg.

The effect of several protease inhibitors on pictobin activity was also examined by determining its activity on DL-BApNA. The purified enzyme (1 μg) was pre-incubated with PMSF, EDTA, TLCK, TPCK, DTT, acetate iodine (IA), 2β-ME, (5 mM each) and SBTI (2 mg/mL) in 50 mM Tris-HCl buffer, pH 7.5, for 15 min at 37 °C.

#### 2.6.2. Fibrinopeptides release

The fibrinopeptides were generated by incubating 1.0 mL of human Fg (3 mg/mL in 0.05 M Tris-HCl buffer, pH 7.4, containing 0.07 M NaCl) with pictobin (4 μg) at 37 °C for 0.1, 1.0, 10, 20 and 60 min. Insoluble proteins were removed with 2% TCA and the fibrinopeptides-containing supernatants were applied to reverse-phase HPLC on an analytical column (4.6 mm × 25 cm) of Vydac $C_{18}$ using a linear gradient (0–15%, v/v, during 15 min; then 15–30% during 60 min) of acetonitrile in 0.1% TFA. Fibrinopeptides A (FPA) and B (FPB) (Sigma) were used as standards.

#### 2.6.3. Fibrino(geno)lytic activity assay

The fibrino(geno)lytic activity was determinate according to [27], by incubating 0.1 mL human Fg (0.2%) with pictobin (3 μg) in 50 mM Tris-HCl (pH 7.4) buffer at 37 °C. Aliquots were taken at 10, 20, 30, 60 and 120 min intervals and separated by SDS-PAGE (12% gels) to examine the cleavage pattern of Fg degradation.

#### 2.6.4. Studies of fibrin clots formation by turbidity and ultrastructural analysis

Fibrin polymerization by pictobin was monitored in low binding polystyrene 96-well plates by the change in turbidity at 405 nm every 15 s for at least 1.5 h at 37 °C using a plate reader according to [28]. Briefly, pictobin (1–10 μg) was incubated at 37 °C for 10 min in the 96-well plates, then Fg (1 mg/mL), preincubated in 25 mM Hepes buffer, pH 7.4, 150 mM NaCl for 10 min at 37 °C was added. Thrombin (0–5 nM) with $CaCl_2$ (5 mM) was used as a positive control.

To analyze the ultrastructural properties of fibrin clots that were generated by pictobin or thrombin were assessed by scanning electron microscopy (SEM), as described: human Fg (5 mg/mL) or citrated human blood were coagulated with pictobin (3 μg) or thrombin (5 U/mL) on microscopy slides. Clots were fixed with 2% glutaraldehyde for 12 h, followed by washing with phosphate buffer and dehydration with an increased alcohol row (20% to 100%). Then, the slides were dried by standardized procedures in the absence of $CO_2$ and clots were coated with plasma gold for 2 min. Fibrin clots were visualized in a FEI Scanning Electron Microscope Model Inspect S50, in a high vacuum mode.

#### 2.6.5. Hydrolytic activity toward chromogenic substrates and kinetic parameters

Pictobin (1 μg) was assayed with various chromogenic substrates: S-2238 (for thrombin), S-2366 (for aPC, XIa), S-2251 (for plasmin) and S-2266 (for glandular kallikrein and factor XIa). Substrates (0.1 mM final concentration) were dissolved in 50 mM Tris-HCl buffer, pH 7.5 containing 150 mM NaCl. The activity was monitored spectrophotometrically at 405 nm using an ELISA System Read Well Touch (Robonik India Pvt. Ltd) at 37 °C for 30 min with repetitive data acquisition at intervals of 5 min. Finally, 10 μL of a 1 mg/mL trypsin solution was added to hydrolyze substrates to completion.

The steady-state parameters $K_M$ and K*cat* were determined as described [26] using the following chromogenic substrates: S-2266, S-2366, D-Phe-Val-Arg-pNa (for thrombin), Bz-Pro-Phe-Arg-pNa (for plasma kallikrein) and S-2251. An appropriate concentration of each substrate was determined by measuring the amount of product released after complete hydrolysis with an excess of trypsin. Reactions were initiated by addition of appropriate amounts of pictobin. The cleavage rate was measured continuously at 410 nm as release of pNA over time. The amount of hydrolyzed substrate was calculated from absorbance at 410 nm by using a molar extinction coefficient of 8800 $M^{-1}$ $cm^{-1}$ for free pNA. The Michaelis Menten constant $K_M$ and $V_{max}$ were calculated by analysis of double-reciprocal plots of initial velocity as a function of the substrate concentration. The substrate with the highest cleavage rate was used for comparative analysis with native and deglycosylated enzyme as well as trypsin and thrombin.

### 2.7. Biological characterization

#### 2.7.1. Platelet aggregation assay

Platelet aggregation was performed with the digital Qualitem aggregometer with AgrePic software. Platelet-rich plasma (PRP) and platelet-poor plasma (PPP) were prepared according to [27]. 300 μL of PRP (3–4 × $10^5$ platelets/μL) were pre-incubated at 37 °C for 1 min,

then 50 μL of pictobin (1, 5, 10, 20, and 40 μg/mL) was added. ADP 20 μM (Sigma, USA) was used as agonist.

*2.7.2. Factor XIII activation*

This test was performed to assess the ability of pictobin to activate factor XIII as described [29]. As positive controls clots produced by thrombin were run in parallel.

*2.7.3. Defibrinating activity*

For this test, a reported protocol to measure defibrination [30] was modified. Briefly, six groups of male Swiss mice (20–22 g, $n = 4$) were injected intraperitoneally with decreasing doses of both, native and deglycosylated enzyme (50, 25, 12.5, 6.0, 3.0, 1.0 μg/mice), in 0.1 mL of saline. Control groups received 0.1 mL of saline. After 2 h, animals were anesthetized, and bled by cardiac puncture. Whole blood was placed in tubes and kept at 25 °C until clotting. The minimum defibrinogenating dose (MDD) was defined as the amount of protein that prevent plasma coagulation after 2 h incubation.

*2.7.4. Edema-inducing and hemorrhagic activity*

Six groups each encompassing four male Balb c mice (18–22 g) were injected with pictobin (25 μL/50 μL PBS) in the subplantar region. As negative control, an equal volume of PBS was injected into the contralateral paw of the mouse. After 3 h, the thickness of the swollen paws was measured with a digital caliper.

Five groups of four male Balb/c mice were used to test hemorrhagic activity according to Kondo et al. [31]. Briefly, the animals received subcutaneous injections of 50 μL of PBS or 50–100 μg of pictobin in the dorsal region. After 2 h injection, mice were sacrificed and the presence of hemorrhagic spots in the inner side of skin was measured with a digital caliper.

*2.8. Effect of plasma inhibitor α2-macroglobulin ($\alpha_2$-M) and heparin*

$\alpha_2$-M was incubated with pictobin at different molar ratios, enzyme:$\alpha_2$-M (1:0.5, 1:1, 1:2, 1:4) in 0.2 M Hepes buffer, pH 7.4 containing 0.15 M NaCl at 37 °C for 5 min. Then, aliquots of each sample were mixed with sample buffer containing SDS and 2β-ME for 30 min at room temperature (RT), boiled 3 min and analyzed by SDS-PAGE (10% gel). Similar samples were used to evaluate the amidolytic, coagulant and fibrinogenolytic activity as described above. For all experiments, two assays were performed: one, pre-incubating pictobin with α2-M, 15 min before assay and without pre-incubation. Heparin at different concentrations (87.5, 175 and 250 IU) were pre-incubated independently with 20 μg enzyme at 37 °C for 30 min and then coagulant activity was evaluated as previously described.

*2.9. Neutralizing studies*

Immunological cross-reactivity of commercial αBS-INS (Peru) and αBS-FUNED (Brazil) with pictobin treated with PNGase-F or untreated enzyme were performed using ELISA [32]. Briefly, multi-well plates were coated overnight with 0.5 μg/well of each protein in 0.05 M carbonate buffer, pH 9.6 (100 μL, standard volume). After washing with 0.05% Tween-saline, blocking solution (2% casein in phosphate buffer saline, PBS) was added (1 h at RT). After two additional washing steps with the same solution, antivenoms diluted in PBS, containing 0.25% casein and 0.05% Tween 20, were added and incubated for 1 h at 37 °C. After six additional washes, peroxidase-coupled anti-horse antibody (Sigma, diluted 1:12000) was added for 1 h at RT. After washing, 100 μL of peroxidase substrate solution containing *o*-phenylenediamine (0.33 mg/mL in citrate buffer, pH 5.2) and 0.04% hydrogen peroxide was added. The color reaction was developed for 1 h at 37 °C in dark. Absorbance was read at 492 nm.

*2.10. Effects on tumor cell lines and mitochondrial functionality*

*2.10.1. Cell culture conditions and cell viability*

Breast cancer MDA-MB-231, lung cancer A549 and HEK293 cells were purchased from American Tissue Culture Collection (ATCC) and were grown in Dulbecco's modified Eagle's medium (DMEM), containing 25 mM glucose and 4 mM glutamine supplemented with 10% fetal bovine serum (FBS), penicillin (100 IU/mL) and streptomycin (100 μg/mL). All culture media contained no exogenous pyruvate supplementation and cells were maintained in a humidified atmosphere at 37 °C and 5% CO2. The viability was determined using the ability of cells to exclude propidium iodide (PI) as described in [33]. In brief, cancer cells were collected from 12-well plates after exposition with PBS (Control) or 5, 10 and 50 μg/mL pictobin for 24 h and the level of PI incorporation was quantified in a BD FACSCanto flow cytometer. PI-negative subpopulations of cancer cells were considered viable.

*2.10.2. Mitochondrial morphology analysis*

To evaluate the mitochondrial morphology, HEK293 cells were transfected with mt-YFP plasmid using lipofectamine 3000 kit (ThermoFisher Scientific). After three days in culture on coverslips, images of mitochondrial morphology were obtained with the following conditions: after basal recording, 50 μg/mL pictobin was added to cells, followed by 1 μM FCCP addition. For cell selection and image acquisition, for each experimental condition 24–26 cells from three different cell cultures were selected. Cells selection was chosen by the following characteristics: high signal-to-noise ratio for mito-YFP, and relative isolation from neighboring YFP from other transfected cells. To analyze and classify mitochondrial morphology, high-magnification images were acquired with an UltraView RS spinning disk microscope (Perkin-Elmer) with a 100× oil objective (NA 1.3, C-Apochromat), excitation with a 488 nm diode laser (Omicron), a 12-bit CCD camera (Hamamatsu ORCA-ER), and Volocity 4.2 software (Improvision). 8-Bit TIFF images of 1344 × 1024 pixels were acquired with 41.5 × 41.5 nm pixel size and 200 nm between z sections. 120–180 z-sections were acquired, depending on cell volume. For the segmentation, high-magnification images were deconvolved with Huygens Scripting software (Scientific Volume Imaging BV) to reduce blurring and noise. Individual cells were selected using eliptic or brush selection using ImageJ software (NIH, USA, http://rsb.info.nih.gov/ij). To mitochondrial segment, we used ImageJ-based MiNA toolkit, following the developer workflow [34,35]. Briefly, 3D images were preprocessed (applied algorithms: Unsharp Mask, CLAHE, Median Filtered), then binary transformed and skeletonized to allow parameters generation and recording.

*2.10.3. Mitochondrial membrane potential ($\Delta\psi m$)*

Cancer cells were grown on coverslips and loaded with 5 nM tetramethylrhodamine methyl ester (TMRM) for 30 min at 37 °C and 5% $CO_2$. The fluorescence in non-quenching mode was acquired using an UltraView RS spinning disk microscope (Perkin-Elmer). A549 cancer cells were exposed to 5, 10 or 50 μg/mL pictobin. To determine the maximal mitochondrial depolarization was added 1 μM FCCP at the end of the experiment. TMRM fluorescence was quantified with ImageJ software.

*2.10.4. NAD(P)H and ROS levels*

Intracellular NAD(P)H levels were measured by auto-fluorescence using excitation and emission wavelengths of 340/428 nm as described [33]. The intracellular ROS levels were measured using dihydroethidium (DHE) probe by flow cytometry as described in Ref. [33]. Antimycin A (1 μM) was used as positive control.

*2.10.5. Determination of ATP levels in glycolytic and oxidative cancer cell subpopulations*

Two subpopulations of A549 cancer cells were grown for 3 days alternatively in a DMEM high glucose medium and galactose (glucose-

free) medium as previously reported by us [33]. The glycolytic and oxidative subpopulations of cancer cells were used to assess the effect of pictobin on glycolytic and mitochondrial contributions to total ATP levels. These cancer cells subpopulations were grown in 96-well plates during 24 h and then, were stimulated with 5, 10 and 50 μg/mL pictobin by 4 h. The ATP levels were determined using CellTiter-Glo Luminescent Cell Viability Assay kit (Promega, USA) as reported [36].

### 2.10.6. Migration assay

Cell migration was evaluated in Boyden Chamber assays (Transwell Costar, 6.5-mm diameter, 8-μm pore size) as previously reported [33]. The MDA-MB-231 and A549 cancer cells were exposure to increasing concentrations of pictobin (5, 10, 50 μg/mL) during 24 h. Then, cancer cells were re-suspended in serum free medium, were plated on top of the chamber insert coated with fibronectin (2 μg/ml) and incubated at 37 °C for 2 h. The inserts were removed, washed and the bottom side of the inserts stained with 0.1% crystal violet in 2% ethanol. Cells from four different frames were counted for each condition in an inverted microscope.

### 2.11. Primary structure and structural modeling of pictobin

We previously reported the nucleotide and deduced amino acid sequences of pictobin [21]. The amino acid sequence, (GenBank: AGZ87932, UniProtKB/Swiss-Prot: U5YCR8) was used for multiple alignment with other homologous sequences employing Clustal X program [37]. Phylogenetic analysis was performed with MEGA program v 7.0 according to the Neighbor-Joining method. Phylogenetic distance was calculated by Kimura method using two parameters and performing 1000 replicates (bootstraps).

To obtain the three-dimensional structure of pictobin, a model was predicted using comparative homology modeling [38]. The pictobin sequence was used as template for BLAST search against the protein database (PDB) to deduce appropriate homologous templates. SV-TLEs from *Agkistrodon c. contortrix* (PDB: 2AIP_A|chain A), AhV_TL-I from *Agkistrodon halys* (PDB: 4E7N|chain A) and Jararacussin-I from *Bothrops jararacussu* (PDB: 4GSO_A|chain A) showing 75%, 72% and 68% identity and 100% query coverage respectively were selected as templates for comparative homology. The selected templates were used to generate 10 models using Modeller 9.16 [39]. The best model was selected from

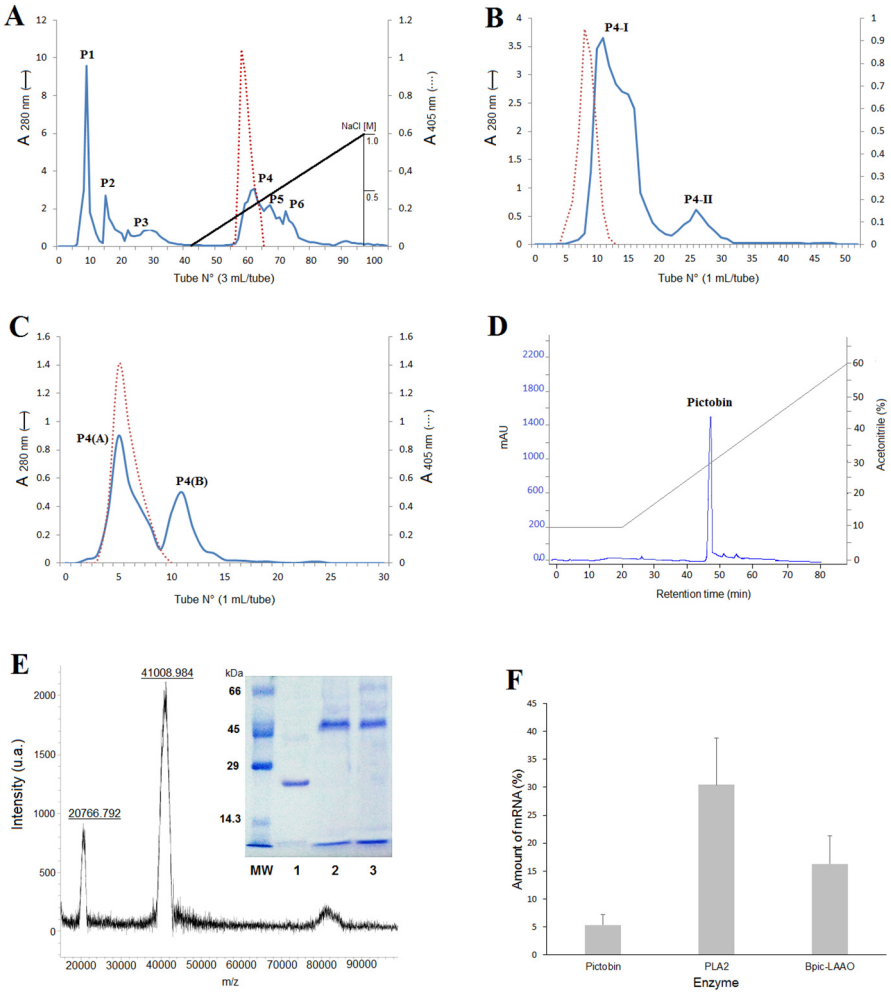


**Fig. 1.** Purification profile of pictobin from *Bothrops pictus* venom. A) Ion-exchange chromatography of crude venom (200 mg) on CM-Sephadex C-50 column, was performed as described in Methods section. Fraction containing TLE activity was polled and concentrated. B) Gel filtration on Sephadex G-100. Fraction from the previous step (33.9 mg) was applied to a gel filtration column as described in Methods section. C) Gel filtration on Sephadex G-75. The active material from the previous step (5.4 mg) was applied on another gel filtration column as described in Methods section. D) RP-HPLC analysis of purified protein obtained from the 3rd step using Vydac $C_{18}$ (4.6 × 250 mm) column, equilibrated with 0.1% TFA in water. Protein was eluted using linear gradient form solution A (0.1%TFA in water) to 100% solution B (0.1% TFA in acetonitrile) for 70 min, at a flow rate of 1 mL/min. E) MALDI-TOF mass spectra and deglycosylation analysis. MS spectrum of pictobin showed a 41,008.984 *m/z* and its doubly-charged (20,766.73 *m/z*) and mono-charged dimer ions (81,487.13 *m/z*). SDS-PAGE (12%, inset) of deglycosylated enzyme, lane 1, pictobin treated with PNGase F; lane 2, pictobin treated with O-glycosidase, and lane 3, untreated pictobin. F) Gene expression analysis by qRT-PCR real time. The levels of expression were determined with respect to the housekeeping GAPDH. The data are presented as mean values ± the standard deviation, $n = 3$, * Levels of significance of control: $p < 0.05$ PLA2: Phospholipase $A_2$, Bpic LAAO: L-amino acid oxidase from *Bothrops pictus* venom.

the least discrete optimized protein energy (DOPE) and modeler objective functions (MOF) scores and carried for further refinement with loop refinement script. The overall and local quality analyses of the final model were assessed by VERIFY3D [40], PROSA [41], ERRAT [42] and PROCHECK [43]. Three-dimensional structures were displayed, analyzed and compared using the program PyMOL v 1.2.8 [44].

### 2.12. Statistical analysis

The enzymatic activity data were expressed as means ± SEM of three independent experiments. Significant differences between treatments were estimated using ANOVA and the Student's *t*-test implemented in the software GraphPad Prism 6.07 (GradPad Software Inc. USA). *P*-values <0.01 ($p < 0.01$) were considered statistically significant.

## 3. Results

### 3.1. Purification of pictobin

Crude venom of *B. pictus* was separated into six peaks by CM-Sephadex C-50 column (Fig. 1A). Peak 4 containing Fg-clotting and amidolytic activity was collected for further purification. The desalted, lyophilized fraction was subjected to gel filtration chromatography on Sephadex G-100 column (Fig. 1B). Two major peaks (P4-I and P4-II) were obtained. The active fractions (P4-I) were concentrated and submitted to another gel filtration on a Sephadex G-75 column (Fig. 1C). The active compound showing Fg-clotting and amidolytic activity was eluted in the first peak (P4A). The homogeneity of the protein was confirmed by reverse phase HPLC and SDS-PAGE (Fig. 1D, E). The purification procedure of pictobin is summarized in Table 1. The final step resulted in an overall yield of 37.9% and a purification factor of 77.7 with respect to amidolytic activity. Purified enzyme represents approx. 0.49% of total venom proteins.

The Mr. of pictobin, determined by mass spectrometry, was 41,008.984 Da (Fig. 1E), it is a single-chain glycoprotein containing approximately 45% carbohydrate. The Mr. was reduced to approx. 27-kDa after digestion with PNGase-F (Fig. 1E, lane 1, inset), whereas its Mr. remained unchanged after treatment with *o*-glycosidase (Fig. 1E, lane 2, inset), indicating that pictobin likely is only N-glycosylated. Pictobin expression represents almost 6% of all transcripts in fresh venom (Fig. 1F), this amount is lower than $PLA_2$s and LAAOs, which are important toxic components of the venom [2–6]. These results partially correlated with the reported venom proteome of *Bothrops pictus*, providing evidence that SVSPs are minor components (7.7%) compared to phospholipases (14.1%) and principally metalloproteinases (68%) [19].

#### 3.1.1. Enzymatic and biochemical properties

Pictobin-mediated clotting of the human and bovine fibrinogen (81 ± 1.3 and 72 ± 1.5 UA/mg protein, respectively), this activity was high as compared to crude venom (Table 2). The MCD upon bovine Fg was determined as 8 μg (Table 2). Likewise, the hydrolysis of BApNA by pictobin was drastically inhibited by PMSF (90%), a specific inhibitor for serine proteases and by the disulfide reducing agents 2-βME (40%) and DTT (38%). Also, SBTI weakly inhibited its amidolytic activity (10%). In contrast, the enzyme was no affected by EDTA, TPCK, TLCK and IA (Fig. 2).

**Table 2**
Pictobin activity upon fibrinogen and plasma.

| | Coagulant activity[a] | | MCD[b] | |
|---|---|---|---|---|
| | Pictobin | Crude venom | Pictobin | Crude venom |
| Fg bovine | 72 ± 1.5 | 23 ± 1.3 | 8 ± 4.35 | 42 ± 1.36 |
| Fg human | 81 ± 1.3 | 35 ± 1.7 | 6 ± 3.45[c] | 49 ± 6.89[c] |
| Human plasma | 60 ± 1.8 | 45 ± 2.1 | 18 ± 6.63[c] | 78 ± 4.89[c] |

The values are shows as mean ± S.D. ($n = 3$).
[a] U.A/mg protein. Expressed as the inverse of the coagulation time per mg of protein.
[b] MCD: minimum coagulant dose. Defined as the amount (μg) of protein that clots 0.2 mL substrate in 60 s.
[c] Date from Vivas et al. 2015.

#### 3.1.2. Effect of pictobin on fibrinogen

The venom proteinase cleaves the Aα-chains of Fg in a highly specific manner by rapidly splitting off FpA as demonstrated by HPLC (Fig. 3). The retention times for standard FpA and FpB (control) are presented in the first panel, however, negligible traces of FpB were detected at 10 min. In addition, pictobin degraded Fg Aα-chains in a time-dependent manner without any significant effect on Bβ- and γ-chains even at 120 min incubation (Fig. 4A). The main degradation product of Fg appeared below the gamma chains at 10 min incubation (Fig. 4A). Fibrin polymerization produced by thrombin and pictobin was compared by analyzing change in turbidity solutions measured by absorbance at 405 nm. As shown (Fig. 4B) pictobin produced lower turbidity than thrombin and reached its maximal value at 30 min. The structure of fibrin clots formed from Fg by both enzymes (Fig. 4C, D) and from blood clots (Fig. 4E, F) were analyzed by SEM. The thrombi

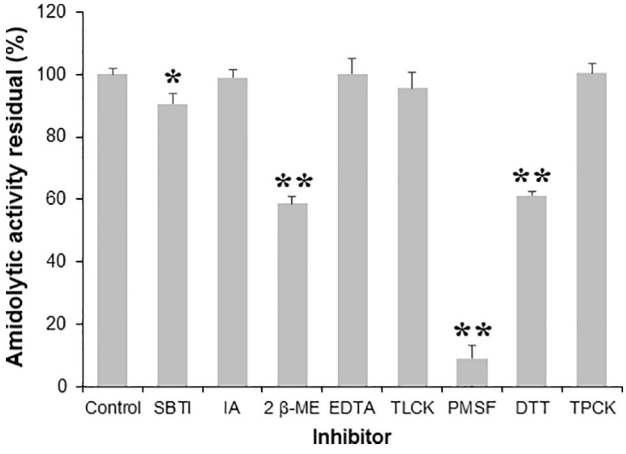


**Fig. 2.** Effect of protease inhibitors on pictobin upon amidolytic activity with DL-BApNA as substrate. SBTI; soybean trypsin inhibitor, IA; iodoacetate, 2β-ME; 2 β mercaptoethanol, EDTA; ethylene diaminetetraacetic acid, TLCK; N-tosyl-lysine chlomethyl ketone, PMSF; phenylmethanethylsulfonyl fluoride, DTT; Dithiothreitol, TPCK; tosyl-L-phenylalanine chloromethyl ketone. Data are expressed as the mean ± S.D. ($n = 3$). Values significantly different from the control: (*) $p < 0.05$, (**) $p < 0.01$.

**Table 1**
Purification scheme of pictobin from *Bothrops pictus* venom.

| Steps | Total protein | | Specific activity[a] (umol/min/mg) | Total activity | Recovery (% initial activity) | Purification (fold) |
|---|---|---|---|---|---|---|
| | (mg) | % | | | | |
| Crude venom | 200 | 100 | 0.017 | 3.4 | 100 | 1 |
| CM-Sephadex C-50 | 33.9 | 16.95 | 0.116 | 3. 3 | 100.0 | 6.82 |
| Sephadex G-100 | 5.4 | 3.2 | 0.651 | 3.51 | 73.23 | 38.29 |
| Sephadex G-75 | 0.981 | 0.49 | 1.321 | 1.29 | 37.9 | 77.7 |

[a] Determinated using DL-BApNA as substrate.

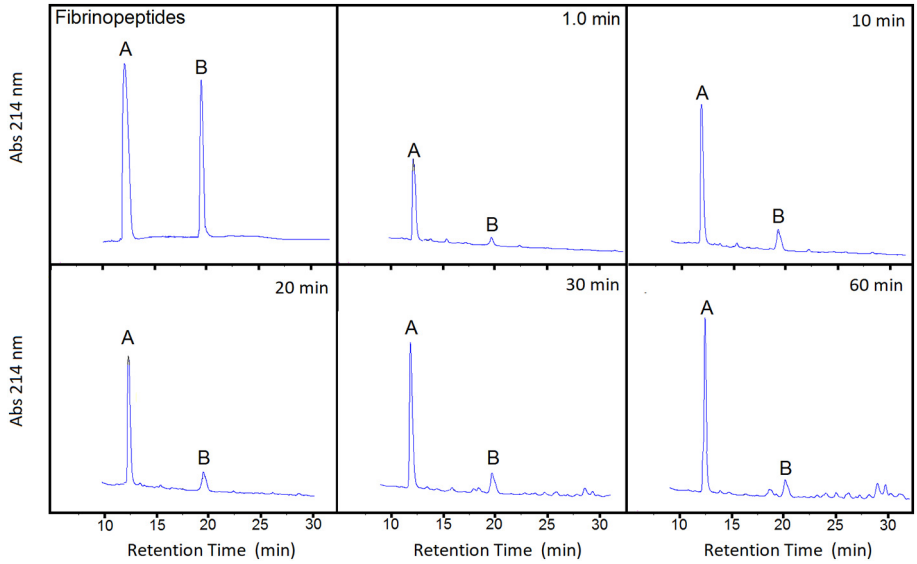


**Fig. 3.** Time-dependent elution profiles on RP-HPLC of peptides released from human Fg by pictobin. First panel, standard fibrinopeptides (Fp) A and B as control, and next panels, time dependent liberation of FPs. Details of conditions are given in the text.

formed by pictobin (Fig. 4D) looked markedly more porous, unstable and translucent than those formed by thrombin (Fig. 4C). In the case of blood thrombi, fibrous/tenuous structures and sheet-like structures were observed as a result of the Fg-clotting enzyme (Fig. 4F), in contrast to the thrombi formed by thrombin (Fig. 4E), Fg-cleavage products were unable to form stable clot. This effect might be caused or reinforced by

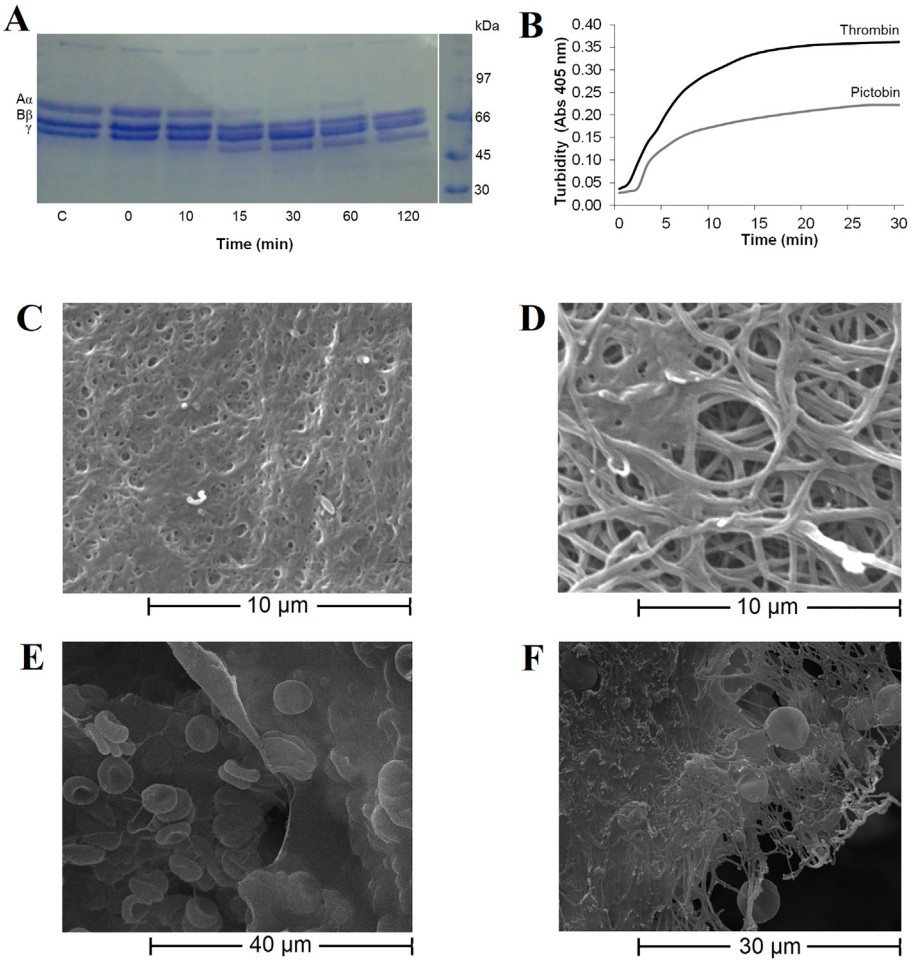


**Fig. 4.** Action of pictobin upon fibrinogen. A) Time course analysis of fibrin(ogeno)lytic activity of pictobin assessed on SDS-PAGE (12%) gel, only the Aα chain was degraded by pictobin. B) Fibrin formation by turbidity assay. Pictobin produces tenuous fibrin polymers than thrombin. C–F) Representative scanning electron micrographs of fibrin and whole blood clots formed by thrombin (C and E) or pictobin (D and F), after 2 h of incubation the enzymes with Fg. Pictobin forms porous/friable fibrin clots compared to thrombin which form compact plates.

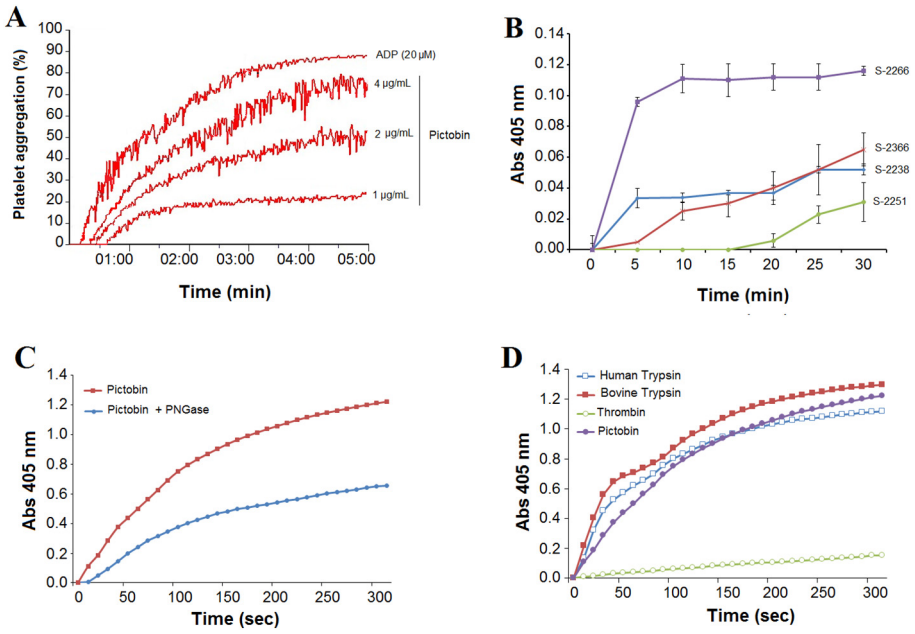


**Fig. 5.** Functional characterization of pictobin. A) Pictobin induces platelet aggregation on human PRP using ADP as agonist (up line). B) Hydrolysis of chromogenic substrates by pictobin was evaluated on: S-2238 (for thrombin), S-2366 (for XIa, aPC), S-2251 (for plasmin) and S-2266 (for glandular kallikrein). C) Pictobin (1 mg/mL), treated with PNGase F (100 U) or untreated enzyme was incubated with S-2266 to assess its amidolytic activity. D) Comparative hydrolysis of S-2266 (0.1 mM) by human and bovine trypsin, human thrombin and pictobin (1 µg/mL each) at 37 °C for 30 min, with lectures at 405 nm at 5 min intervals. The values are expressed as absorbance units and are shown as means ± S.D., $n = 3$.

the fact that pictobin did not activate factor XIII. The resulting absence of isopeptide crosslinkages left the fibrin bundles left further unstabilized and allowed quick dissolution of the pictobin-induced clot by urea solution (a standard assay for the presence of activated factor XIII, not shown).

### 3.1.3. Effect on platelet aggregation and chromogenic substrates

Pictobin induced aggregation on human platelet rich plasma (PRP) in a dose-dependent manner (Fig. 5A). Pre-incubation with PMSF did not alter the aggregation induced by the enzyme (not shown), ruling out that its catalytic activity is involved in platelet activation or aggregation.

Fig. 5B, shows the relative hydrolyzing activity of pictobin toward several chromogenic substrates. The enzyme efficiently hydrolyzed the substrate for glandular kallikrein, S-2266 in 10 min, whereas the thrombin substrates S-2366 and S-2238 were partially degraded. However, the plasmin substrate S-2251 with basic amino acid residue Lys in place of Arg at P1 site was not efficiently hydrolyzed. Table 3 shows the kinetic parameters of pictobin on several chromogenic substrates. The substrates for kallikrein, D-Val-Leu-Arg-pNa (S-2266) and D-Pro-Leu-Arg-pNA (S-2366), both containing hydrophobic residues at the P2 and P3 site, were the most sensitive for pictobin with regards to the catalytic efficiency ($k_{cat}/K_M$). The kallikrein substrate (S-2266) was the best for pictobin, and its catalytic conversion was similar to the ones by human and bovine trypsin, but not by thrombin (Fig. 5B and D). Enzymatic activity of pictobin depended on the presence of its glycoconjugates, as its amidolytic activity on the best substrate S-2266, decreased to approximately 50% after its deglycosylation with PNGase F (Fig. 5C).

### 3.1.4. Biological properties

The enzyme induced defibrination in mice, thereby preventing blood coagulation after two hours injection. The estimated minimum defibrinogenating dose (MDD) was 0.02 mg/kg. Importantly, after treatment with PNGase F, the enzyme lost its defibrinogenating effect (not shown). This suggests the important role of carbohydrate moieties to modulate the physicochemical properties and to improve its catalytic activity. In addition, pictobin showed low edema-inducing effect (0.15 mg/kg) compared with that induced by the whole *B. pictus* venom, and was devoid of both myotoxic and hemorrhagic activity (data not shown).

### 3.1.5. Effect of heparin, α 2- Macroglobulin and cross-reactivity with bothropic antivenoms

Interaction of pictobin with the main plasma protease inhibitor α2-M (720-kDa) was analyzed by SDS-PAGE after incubating pictobin with α2-M at molar ratios enzyme: inhibitor of 1:0.5, 1:1, 1:2 and 1:4. Under reduced conditions, the 180-kDa α2-M sub-units were cleaved to a 90-kDa fragment in a concentration dependent fashion as shown in Fig. 6A. Furthermore, its amidolytic activity was significantly reduced when α2-M was pre-incubated with enzyme for 15 min. However, no significant inhibition was detected if pictobin and the inhibitor were mixed together and added to the substrate (Fig. 6B). Similar results were obtained with its fibrinogenolytic activity (Fig. 6C), as pre-incubation of

**Table 3**
Kinetic parameters for the hydrolysis of peptidyl p-nitroanilides by pictobin.

| Substrates | $K_M$ (µM) | $V_m$ (µM/s) | kcat ($s^{-1}$) | $kcat/K_M$ ($s^{-1}/µM^{-1}$) |
|---|---|---|---|---|
| D-Val-Leu-Arg-pNa[a] | 2.23 ± 0.163 | 2.09 ± 0.08 | 10.32 | 4.63 |
| D-Pro-Leu-Arg-pNa | 2.98 ± 0.134 | 0.02 ± 0.006 | 11.2 | 3.74 |
| D-Phe-Val-Arg-pNa | 11.69 ± 0.458 | 2.29 ± 0.08 | 11.34 | 0.97 |
| Bz-Pro-Phe Arg-pNa | 5.44 ± 0.551 | 0.46 ± 0.01 | 2.30 | 0.42 |
| D-Val-Leu-Lys-pNa | 7.55 ± 0.513 | 0 0.01 ± 0.77 | 0.17 | 0.02 |

The values are shows as mean ± S.D. ($n = 3$).
[a] The best substrate.

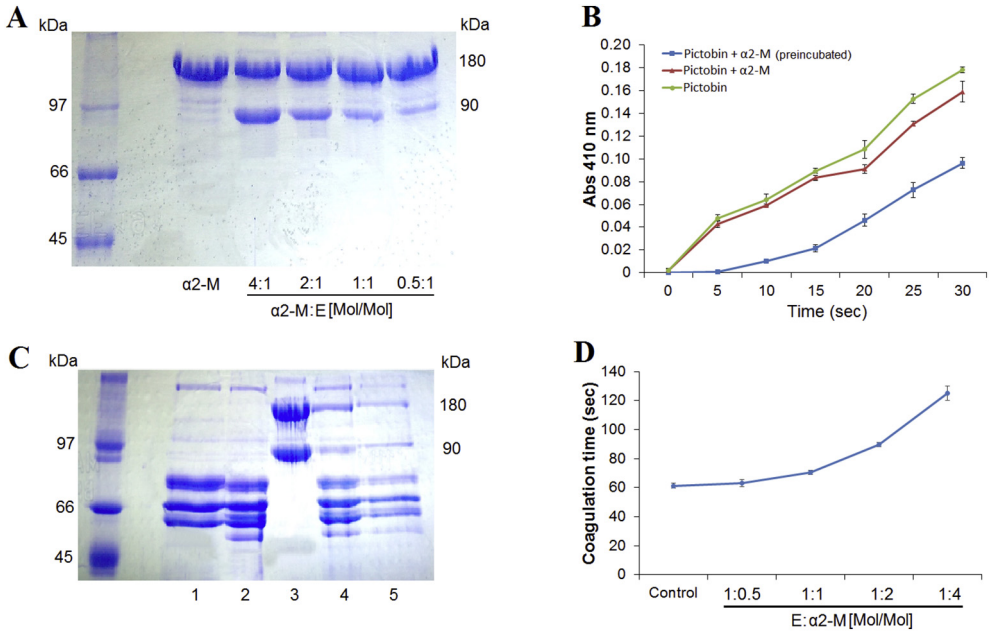


**Fig. 6.** Interaction of α2-Macroglobulin with pictobin. A) SDS-PAGE (12%) gel after incubation α2 M with pictobin at several molar: ratios of α2-M:enzyme. B) Amidolytic activity upon S-2266, using inhibitor:enzyme, incubated at 37 °C for 15 min or both samples added together. The absorbance was decreased when the enzyme and inhibitor were pre-incubated. C) Fibrin(ogen)olytic assay, lane 1: Fg (0.4 mg), lane 2: Fg + pictobin (2 μg), lane 3: α2M + pictobin [mol/mol], lane 4: Fg + α2M + pictobin and lane 5: Fg + (pre-incubated α2M + pictobin). α2-M blocked the Fg Aα-chains cleavage by pictobin, compared to control (lane 2). D) Effect of α-2 M on coagulant activity induced by pictobin, one DCM-F of pictobin (6 μg) was tested on coagulation in presence of α2-M, using the molar ratios of, E: α2M: 1:0.5, 1:1, 1:2 and 1:4. In B and D, the values are expressed as means ± S.D., ($n = 3$).

enzyme with its inhibitor, resulted in slight decrease of Fg Aα chains (line 4 and 5) in comparison to Fg control (line 1). As Fg is the precursor of fibrin and a mediator of platelet aggregation it plays a central role in coagulation and hemostasis. Thus, we have evaluated the coagulation time of Fg in presence of pictobin treated with α-2 M at molar ratios E:I of 1:0.5, 1:1, 1:2 and 1:4. As can be seen (Fig. 6D), complexation of pictobin with α-2 M at molar ratios above 1:1 of E:α2-M, resulted in a prolonged coagulation time *in vitro*. Inhibition of pictobin by α2-M could be the result of steric hindrance, since the subunits of α2-M (180 k-Da) were slowly cleaved by the enzyme in the bait region to generate 90-kDa fragments. Similarly, to most SV-TLEs, coagulant activity of pictobin was insensitive to heparin even at doses of 87.1 to 171 UI (Fig. 7A). Unlike thrombin, this data suggested that pictobin did not interact with the substrate exosite II (heparin-binding site). With respect

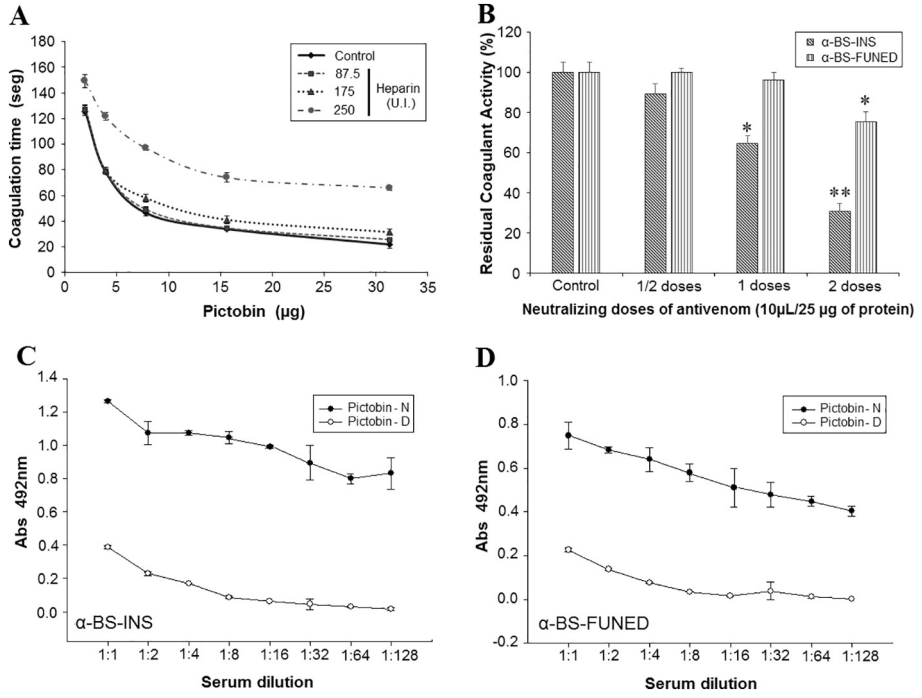


**Fig. 7.** Effect of heparin on coagulant activity and cross-reactivity of pictobin with Peruvian and Brazilian commercial antivenoms. A) Coagulant activity of pictobin was not affected by heparin, conditions are described in Methods section. (B) Coagulant activity was neutralized by commercial *Bothrops* antivenom (α-BS) from INS and FUNED, (C, D) Cross-reactivity of pictobin treated with PNGase-F or untreated enzyme with therapeutic αBS of INS or FUNED. Experimental conditions are described in Materials and methods. Each point represents mean ± SD of two experiments in triplicate.

to anti sera against snake venoms, Peruvian α-BS-INS was more effective in neutralizing the coagulant activity of pictobin than the Brazilian α-BS-FUNED (Fig. 7B). This may be explained by the fact that venom of *B. pictus* was included in the antigenic pool to prepare the therapeutic α-BSA-INS. ELISA assays using pictobin treated with PNGase-F or untreated enzyme showed that the deglycosylated enzyme lost drastically its reactivity with both anti-venoms (Fig. 7C, D). These results demonstrate the relevant role of N-linked glycans to maintain the neutralizing effect of therapeutic antivenoms. Moreover, as the antivenoms were unlikely directed to the N-glycoconjugates, the decreased immunologic reaction of deglycosylated pictobin suggested that deglycosylation destabilized the three-dimensional folding of pictobin and consequently caused the loss of structural epitopes. To our knowledge most SVSPs contain carbohydrates at variant glycosylation sites, that stabilize the catalytic efficiency as well as their interaction with some inhibitors and substrates [7].

### 3.1.6. Effect of pictobin on viability and migration of cancer cells

The breast and lung cancer cells were exposed at increasing concentrations of pictobin by 24 h and the effect on viability was measured. As Fig. 8A–B shows, pictobin did not influence viability of MDA-MB-231 and A549 cancer cells. Interestingly, pictobin reduced the fibronectin-dependent migration in a doses-dependent manner in both cancer cell lines (Fig. 8C–F).

### 3.1.7. Effect of pictobin on cellular metabolism and mitochondrial bioenergetics

In order to explore the effect of pictobin on mitochondrial bioenergetics, pictobin or FCCP, a known protonophore uncoupler of oxidative phosphorylation (OXPHOS), were alternatively added to A549 cells and NAD(P)H levels were measured. As Fig. 9A shows, FCCP promoted an increase of NAD(P)H oxidation and antimycin A, a respiratory complex III inhibitor, produced accumulation of NADH in A549 cancer cells, which was consistent with our previous reports [33]. Pictobin produced a major increase of NAD+ levels close to 70% than FCCP (close to 48%), while antimycin has a minor effect on NADH accumulation (Fig. 9A). Similar effects were observed on NAD(P)H levels of MDA-MB-231 and MCF7 breast cancer cells (data not shown). In addition, pictobin produced Δψm decrease in a concentration-dependent manner (Fig. 9B) without effects on intracellular ROS production (Fig. 9C).

To evaluate if pictobin affects the cellular metabolism, altering the energy production by glycolysis and mitochondria, A549 cancer cell subpopulations with bioenergetic phenotype based on glycolysis or OXPHOS were generated and confirmed by treatment with 1 μM oligomycin (an ATP synthase inhibitor). In oxidative subpopulation,

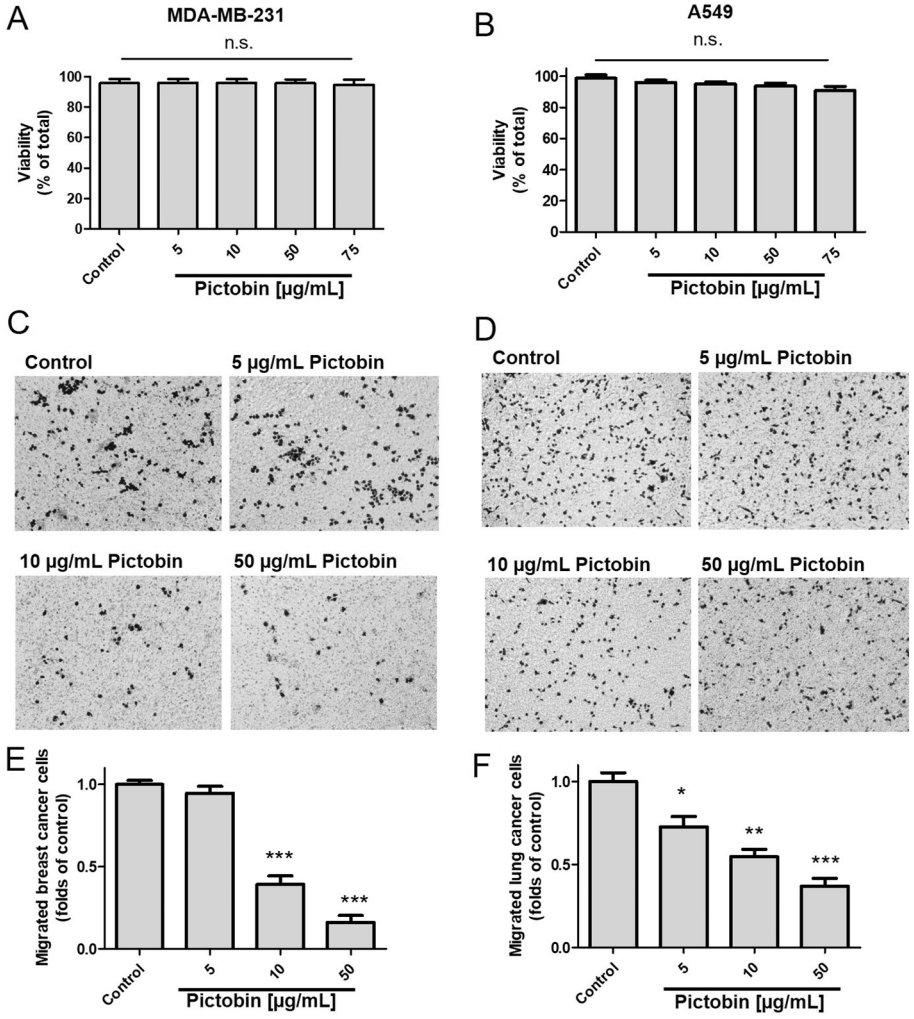


**Fig. 8.** Pictobin has migrastatic effect on breast and lung cancer cells. A–B) Effect of pictobin on viability of breast MDA-MB-231 and lung A549 cancer cells at 24 h of exposure, using PI assay by flow cytometry. C–F) Effect of pictobin on fibronectin-dependent migration of cancer cells. Cells were incubated for 24 h and then, transwell assay were done by 2 h. Details in Material and Methods section. Data shown are the mean ± SD of three independent experiments. *p < 0.05, **p < 0.01, ***p < 0.001, *vs.* Control (PBS). n.s.: not significant.

the ATP levels were significantly decreased by oligomycin, suggesting that OXPHOS is essential in the energetic maintenance (Fig. 9D). In contrast, glycolytic subpopulation exhibited non-significant changes in the ATP levels in presence of oligomycin (Fig. 9D). Using these two cell subpopulations, the effect of pictobin on ATP levels were determined. As Fig. 9E shows, the ATP levels of the oxidative subpopulations were significantly reduced at 2 and 4 h of exposure with pictobin. In contrast, glycolytic subpopulations slightly decreased the ATP levels at 4 h of exposition to 50 μg/mL pictobin. All data suggest that pictobin is a toxin that decreases the mitochondrial bioenergetics.

### 3.1.8. Effect of pictobin on mitochondrial morphology

Alterations in the mitochondrial bioenergetics produce changes in the mitochondrial morphology and dynamics [45]. We hypothesized that inhibition of mitochondrial bioenergetics by pictobin promotes changes in the mitochondrial network. The 3D reconstruction shows

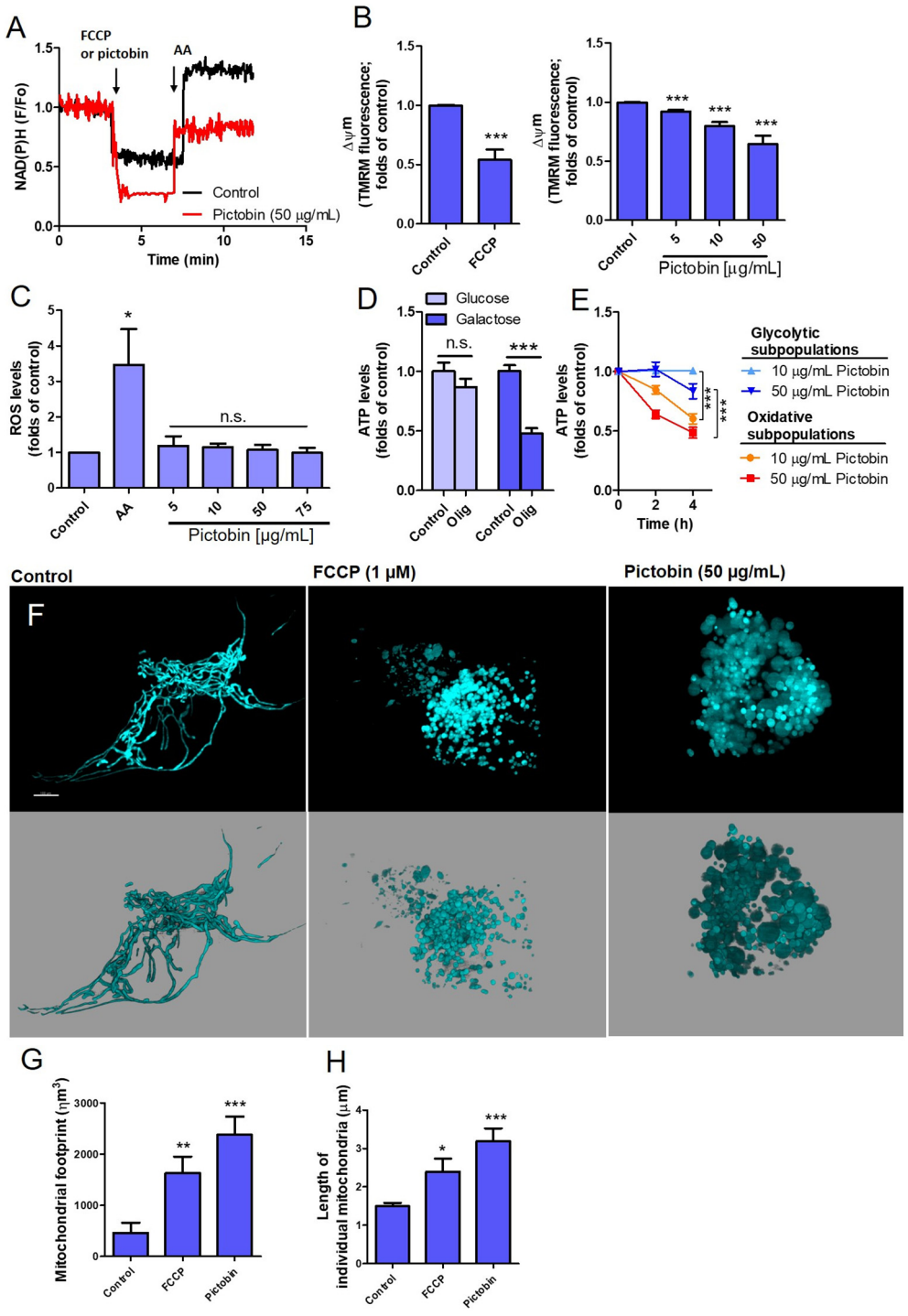


**Fig. 9.** Pictobin produces mitochondrial dysfunction. A) Pictobin (50 μg/mL) induces mitochondrial NADH oxidation in A549 cells. B) Pictobin produces concentration-dependent mitochondrial depolarization in A549 cells. C) Effect of pictobin on intracellular ROS levels in A549 cells at 2 h of exposure. D–E) Effect of 1 μM oligomycin (olig) and pictobin on ATP levels of glycolytic and oxidative subpopulations of A549 cells. Experimental conditions are described in Materials and Methods. F–H) Effect of pictobin (50 μg/mL) on mitochondrial morphology in HEK293 cells transfected with mito-YFP. FCCP (1 μM) was used as positive control of mitochondrial fragmentation. Experimental conditions and image analysis are described in Materials and Methods Data shown are the mean ± SD of three independent experiments. *$p < 0.05$, **$p < 0.01$, ***$p < 0.001$, *vs.* Control (DMSO). n.s.: not significant.

that HEK293 cells transfected with mito-YFP treated with vehicle (PBS), FCCP or pictobin for 4 h had different mitochondrial morphology. Both FCCP and pictobin promoted extensive fragmentation of mitochondrial network compared with the Control (Fig. 9F), which it exhibited a mitochondrial morphology larger and more extensively branched with scarce individual (round and punctate) mitochondria (Fig. 9F). The pictobin-induced morphological changes were characterized by an increase in mitochondrial footprint, suggesting a mitochondrial

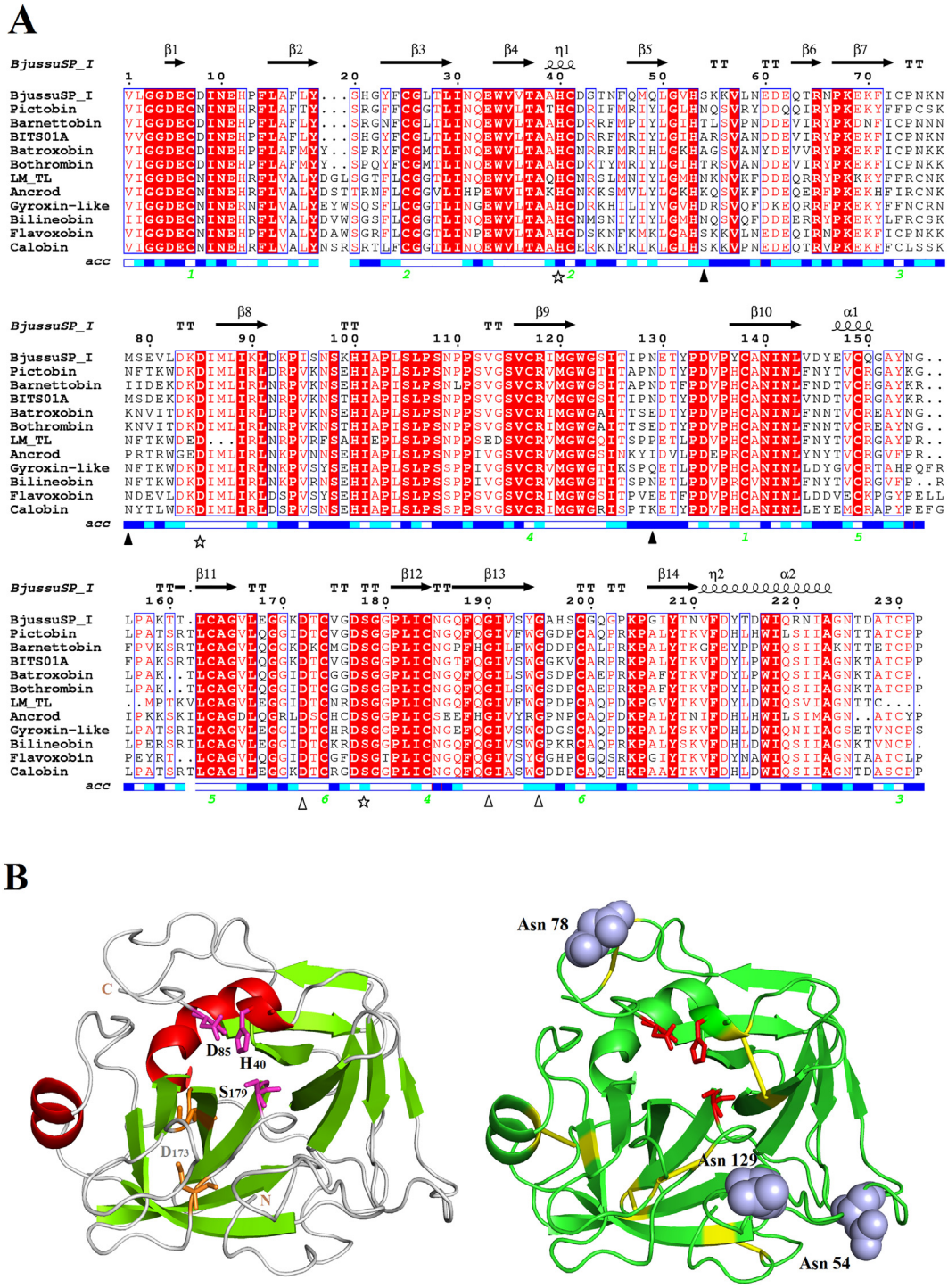


**Fig. 10.** A) Multiple alignment of pictobin with the sequences of other snake venom clotting serine proteases. The red colored residues show the conserved regions throughout. The residues were numbers in alignment to BjussuSP_I and its secondary structural elements. The catalytic triad residues ($H_{40}$, $D_{85}$, $S_{179}$) are marked with a starts. Specificity sites S1 ($D_{73}$), S2 ($G_{91}$) and S3 ($G_{96}$) are in (Δ). Cys-Cys bonds are showed with green numbers. The asparagines for N glycosylation motif Asn-aaX-Ser/Thr are marked with (▼). Sequences were from the following sources: Barnettobin (*B. barnetti*: AFV08640), BjussuSP_I (*B. jararacussu*: ABC24687), Batroxobin (*B. atrox*: P04971), BITS01A (*B. insularis*: Q8QG86), Bothrombin (*B. jararaca*: P81661) LM-TL (*L. muta*: 1919267A), Ancrod (*A. rhodostoma*: AAA49195), Gyroxin (*C. durissus terrificus*: Q58G94), Bilineobin (*A. bilineatus*: Q9PSN3), Flavoxobin (*T. flavoviridis*: P05620) and Calobin (*A. caliginosus*: Q91053). Surface accessibility is depicted for modeled regions with white, cyan, blue and red color for buried, intermediated, accessible residues and incomputable residues respectively. Figure was generated with ESPript server. B) Left: Final theoretical pictobin cartoon model showing the disposition of the catalytic triad (His40, Asp85, and Ser179) (red sticks) and the disulfide bridges (yellow sticks). Right: Theoretical pictobin cartoon model showing the catalytic residues (red sticks) and the predicted N-linked oligosaccharides sites (Asn54, Asn78 and Asn129) (blue spheres). Generated by the program PyMOL.

swelling (Fig. 9G), and increased length of individual mitochondria (Fig. 9H), which were large/rounded and without branches. These results indicate that pictobin induces a dysfunctional bioenergetic status with fragmented mitochondrial network.

### 3.1.9. Molecular characterization of pictobin

We previously reported a cDNA of 754 bp codifying a mature protein with 233 amino acid residues and a fragment of 11-amino acid signal peptide followed of six residues (QKSSEL) of activation peptide [21]. The multiple sequence alignment of mature pictobin with other homologous SV-TLEs (Fig. 10A) showed the essential residues in conserved position such as (according pictobin numbering): His40, Asp85 and Ser179 (catalytic triad); Asp173, Gly191 and Gly196 (substrate-binding sites S1, S2 and S3, respectively); twelve Cys residues (in 7, 25, 41, 75,117, 138, 149, 164, 175, 185, 200 and 231 positions) that formed six disulfide bridges. Additionally, the primary structure included the zymogen activation motif (Gly121, Trp122, and Gly123), $Na^+$ binding region (Pro119, Cys200. Ala201, Gln202, Pro203, Arg204, Lys205, and Pro206) and the hydrophobic site (Tyr39, Phe79, Trp82, Tyr153, Phe194 and Trp195). Among the five potential N-glycosylation sites that were identified (Asn54, Asn78, Asn129, Asn146 and Asn226), only Asn54, Asn78 and Asn129 (Fig. 10B) had the highest likelihood to serve as presumptive glycosylation motif according to the program NetNglyc. The predicted glycosylation sites are near the catalytic pocket, which agree with the role of deglycosylation in stability and enzymatic activity.

### 3.1.10. 3D model of pictobin and phylogenetic tree of SVSPs

The putative 3D model of pictobin (Fig. 10B) was generated according to knowledge-based homology modeling using crystallographic structure of SV-TLE from *Agkistrodon c. contortrix* (PDB: 2AIP_A) as template (75% identity, 93% sequence coverage and a root mean square deviation of 0.2). The generated model showed good stereochemistry quality with 98% of its amino acid residues in the core and additionally allowed regions of Ramachandran plot. The structural modeling showed a quality resolution of 93.21% and 91.53% by using PROCHECK and VERIFY3D software respectively. The PROSA analysis indicated a *Z*-Score of – 8.45. The overall structure of pictobin was composed of twelve beta barrels and four alpha helices (Fig. 10B) typical of a β/β hydrolase. The spatial organization of the catalytic triad residues H40, D85 and S179 at the active site cleft is between the two subdomains of the β-barrel structure and it is surrounded by various loops (Fig. 10B).

A phylogenetic tree was constructed from the sequences of a group of SVSPs including thrombin and trypsin with the aim to analyze the evolutionary relationship among these proteases (Fig. 11). It supported a putative monophyletic clade of SVSPs containing three functionally subclades/subtypes: clotting enzymes (CLs), kininogenases (KNs) and the plasminogen activators (PAs). Snake venom gland serine proteases, such as the clade of clotting enzymes (SV-TLEs) had diverged from glandular kallikrein [42]. In line with this, all data reported so far suggested that the amino acid sequences of the venom gland serine proteases had diverged in an accelerated manner and that their functions had altered in an independent way [9,46,47].

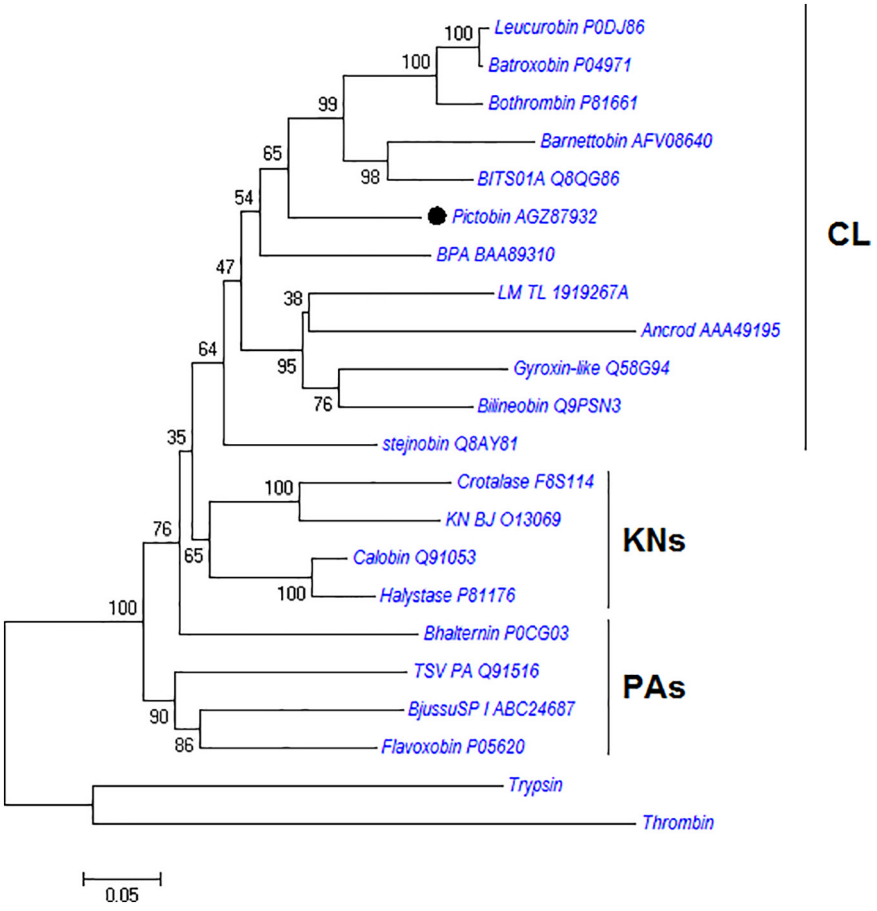


**Fig. 11.** Phylogenetic tree of pictobin with other serine proteases. The evolutionary history was inferred using the Neighbor-joining method. Phylogenetic analyses were conducted using MEGA 6. Evolutionary distances were computed using the JTT matrix-based method. The number indicate the MEGA 6 bootstrap test (2000 replicates). Gen Bank code are show side the enzyme names. The enzyme abbreviations additional to Fig. 10A are: halystase (*G. blomhoffii*), stejnobin (*T. stejnegeri*), LV-PA (*L. m. muta*,), TSV-PA (*T. stejnegeri*), KN-BJ (*B. jararaca*). CLs: coagulating enzymes, KNs: kininogenases, PAs: plasminogen activators.

## 4. Discussion

The fibrino(geno)lytic enzymes including serine and metalloproteinases are widely distributed in several South American pit viper venoms. They lead to spectacular changes in physiological process in hemostasis, in the kallikrein-kinin system and in vascular integrity. Their principal targets are Fg, prothrombin and factor X [19,29,48]. This article reports the structural and functional properties of the Fg-clotting (SV-TLE), pictobin previously isolated from Peruvian *B. pictus* snake venom [21]. It is a highly glycosylated (45%) proteinase similar to other homologous SVSPs such as BPA (62%) from *B. jararaca* [48], barnettobin (45%) from *B. barnetti* [25] and BJ-48 (42%) from *B. jararacussu* [24]. Fg-clotting enzymes are single chain glycoproteins with molecular weights varying from 26 to 67 kDa, depending on their carbohydrate content [7]. Glycoconjugates consisting of *N*-acetyl-D-glucosamine (NAG), fucose, sialic acid, hexose, *N*-acetyl-neuraminic acid, galactose and mannose are frequently reported [10]. To our knowledge the carbohydrate moieties are relevant to modulate the physicochemical properties and for structural stabilization of the SVSPs [48]. In addition, the different levels of glycosylation or other post-translational modifications during the synthesis of SVSPs in the venom gland, are responsible for the microheterogeneity of these proteins [49–52]. Concerned with the efficacy of the therapeutic bothropic antivenoms (αBS) produced at INS-Peru and FUNED-Brazil, we have evaluated the immunological properties of these αBS in neutralizing the main activities of the enzyme. As shown in Fig. 7, the glycosylation on the molecule may have a great influence in the interaction with the antivenoms to neutralize the catalytic effects of pictobin. In this regard, ELISA tests revealed that both αBS displayed strong immunological cross-reaction against pictobin. This may be explained by the presence of common/conserved epitopes in the SV-TLEs. Furthermore, we previously reported that both therapeutic αBS efficiently neutralize the toxicity of predominant compounds including SVMPs, L-amino acid oxidases, $PLA_2$s and Fg-clotting enzymes of several *Bothrops* venoms [32].

The term of thrombin-like enzymes as applied to venom proteases generally implies only the capacity to clot Fg *in vitro*. But, *in vivo*, they function as anticoagulants. Hence, they are intermediate between true coagulants and anticoagulants factors, sometimes called pseudo-coagulants. In accordance with this, pictobin preferentially cleaves Fg α-chains releasing FpA that frequently leads to the formation of a friable fibrin clot that have different mechanical properties, distinct from a clot of thrombin-cleaved fibrin, as we demonstrated by turbidity test (Fig. 4B) and electron microscopy (Fig. 4C–F). Thus, this kind of thrombi is readily dispersed by the normal fibrinolytic system. Based on these unique properties, other Fg-clotting enzymes, *e.g.* ancrod (Arvin™, Knoll, Ludwigshafen, Germany) purified from *Calloselasma rhodostoma* (formerly *Agkistrodon rhodostoma*) and batroxobin (Defibrase™, Reptilase™, Pentapharm, Basel, Switzerland) from *B. atrox*/*B.a. moogeni* have been harnessed for clinical use as defibrinogenating agents [52,53]. Like other SV-TLEs, this effect is facilitated by the fact that most coagulating enzymes do not activate factor XIII and are not susceptible to inhibition by plasma inhibitors, *e.g.* antithrombin [2,5–7]. In this regard, the defibrinogenating action also reduces blood viscosity and produces a consumptive coagulopathy thereby improving blood flow characteristics [54]. Moreover, pictobin induced platelet aggregation in human PRP in a dose-dependent fashion similar to PA-BJ, acutin, thrombocytin and batroxobin [55–57]. Also, pictobin efficiently hydrolyzed specific substrates for kallikrein (S-2266 and S2302) indicating a preference for Arg residue in P1 substrate position [26,58,59]. Our data on $Kcat/K_M$ ratios indicates the influence of residues in P2 (L-Leu) and P3 (D-Val) on hydrolysis rate of Arg-pNA bond [58]. This remark confirmed the specificity of pictobin to Arg-Gly bond in Aα-chain of Fg. The action on kallikrein substrates suggested that pictobin may induce kinin release with an additional hypotensive and intravascular effect during envenomation similar to leucurobin, crotalase and batroxobin [26,58].

In the blood, α2-M regulates the activity of endoproteinases mainly by clearing them from circulation, rather than by inhibition. It has been shown [60,61], that the interaction of a number of proteinases with α2-M involves the cleavage on the α2-M "bit region" by a protease suggesting that the plasma inhibitor was a good substrate [60]. Under our experimental conditions, the quarter (180-kDa) subunits of α2-M were susceptible to proteolytic cleavage, to yield products of ~90-kDa. Hydrolysis of Fg α-chain by pictobin was slightly affected in the presence of α2-M, probably as a result of steric hindrance as reported for other proteolytic enzymes [60,61], but different for other SV-TLEs *e.g.* the enzyme purified from *Lachesis muta muta* [62]. However, α2-M does not affect the hydrolysis of the small chromogenic substrate S-2266. These differences are probably due to substrate size; small substrates have easier access to the catalytic site although an inhibitor is present [61,63]. Furthermore, the coagulant effect of pictobin was delayed by α2-M at molar ratios E:α2-M above 1:1. These findings are in agreement with the differences previously reported in MCD values between citrated plasma that contains α2-M (18 μg) and purified Fg (6 μg) [21], which were similar to those reported for several *Bothrops* venoms [32]. Few Fg-clotting enzymes including ancrod, batroxobin and gabonase have been reported to interact with α-2M [1], but the details of this inhibition process is still elusive.

The hydrophobic sites and other characteristic elements of secondary structure (α-helices, β-strand and loops) are conserved in pictobin. Similarly to other SV-TLEs there are highly conserved residues at regions 1–19, 23–44, 82–91, 97–107, 108–127, 132–153, 156–170, 178–190 and 199–233, in line with a recent report [10]. The presence of a proline at position 206 prevents allosteric regulation by sodium ion on pictobin activity [49], this characteristic has been demonstrated experimentally [21] and is consistent with most SV-TLEs [10]. In thrombin, which is allosterically regulated by the sodium ion, this position is occupied by tyrosine [64]. A Gly177 in pictobin allows a weak interaction with the trypsin inhibitor as evidenced in inhibition assay. Finally, the Thr174 residue enables pictobin to interact with the synthetic substrates BApNA and TAME [65].

The heterogeneous composition of a solid tumor is caused by cancer cell subpopulations with different tumorigenic properties and confers variability in their proliferative capacities and survival advantages [66]. Notably, the rewiring of metabolism and mitochondrial bioenergetics support the high demand for ATP and metabolic intermediates required for the synthesis of DNA and macromolecules during proliferation and metastasis in cancer cells [67,68]. In this work, we describe that pictobin lacks cytotoxic effect but inhibits the fibronectin-stimulated migration in breast and lung cancer cells, an oxidative metabolism-dependent process [69,70]. Moreover, this protease increases NADH oxidation, mitochondrial depolarization, inhibition of mitochondrial ATP synthesis and promotes a metabolic phenotype with fragmented mitochondria. To our knowledge, this is the first report of a coagulating snake venom proteinase that triggers mitochondrial dysfunction at non-cytotoxic concentrations. Given that pictobin possesses glycosylations that maintain the protease activity, we hypothesize that this enzyme is unable to be internalized in cells and to act directly on mitochondria as other snake venom toxins [71–73]. In analogy to the mitochondrial effects of pictobin described here, human thrombin was reported to enhance the mitochondrial energetic metabolism during platelet activation by intracellular signaling dependent on platelet membrane glycoprotein GPIb activation/cleavage, involving PI3K/Akt and calcium mobilization [74]. Similarly, pictobin-induced mitochondrial dysfunction may be triggered by an intracellular signaling initiated in the plasma membrane by cleavage of some receptor in cancer cells. Further studies to understand this novel mechanism of pictobin will be required.

The overall structure of pictobin showed the typical fold of a trypsin-like serine protease: the residues of the catalytic site are located between the two six-stranded β-barrels. Six disulfide bridges that are similar to other SVSPs [9,10,24] stabilizes the structure of pictobin. The 3D

structure of SVTLEs is divided into two subdomains namely, N- and C-terminal domains [10]. The catalytically active residues, His40 and Asp85 are located in the N-terminal region and the Ser179 in the C-terminal subdomain. In addition, the catalytic pocket of pictobin is surrounded by loops that are involved in the recognition of specific substrates and its susceptibility to inhibitors [10,24]. These loops harbor the residues 37, 60, 70, 99, 148, 174 and 218 [49]. In case of pictobin the loop 99 is more open and probably exert influence in the interaction with some inhibitor such as α2-M.

The phylogenetic analysis (Fig. 11) shows three independent and parallel evolutionary clades of SVSPs: the clade of the coagulating enzyme (CL), the kininogenase (KN) and the plasminogen activator (PA). These enzymes are highly homologous in sequence, composed by approximately 233 amino acid residues with multifunctional properties. They have diverged from a common ancestral molecule [46]. According to this hypothesis, the snake venom gland serine proteases, such as pictobin have diverged from glandular kallikrein and their biological functions have altered during evolution. This functional diversity is given by genetic events such as gene duplication, accelerated point mutations [46], and the accelerated segment switch in exons to alter targeting (ASSET) [47]. These gene events confer new enzymatic and functional activities on conserved structural folds, which is common among venom proteins.

In conclusions, this work has clarified the main structural and biochemical properties of the major Fg-clotting enzyme, pictobin of *B. pictus*, an endemic Peruvian pit viper snake. Its cleaving activity toward fibrinogen α-chains may gradually affect the coagulation cascade. The high content of carbohydrate has important role on the structure of its active site, thereby to enhance its catalytic activity and may be involved in the enzyme-inhibitor interactions. Moreover, the N-linked glycans have relevant role in cross-reactivity with therapeutic *Bothrops* antivenom (αBS). In addition to its defibrinogenating effect in *in vivo* models, pictobin alters the mitochondrial function and network of the tested tumor lines as well as their *in vitro* migratory capacity. All these data provide a rational foundation to explore the therapeutic potential as anti-thrombotic and anti- metastatic agent.

## CRediT authorship contribution statement

**Dan E. Vivas-Ruiz:**Conceptualization, Methodology, Investigation, Writing - original draft, Resources, Visualization.**Gustavo A. Sandoval:** Investigation, Resources, Writing - original draft.**Edgar Gonzalez-Kozlova:**Investigation, Formal analysis, Visualization.**Jacquelyne Zarria-Romero:**Methodology, Resources, Investigation.**Fanny Lazo:**Investigation, Validation.**Edith Rodríguez:**Investigation, Validation. **Henrique P.B. Magalhães:**Investigation, Resources, Writing - review & editing.**Carlos Chávez-Olortegui:**Resources, Writing - review & editing, Funding acquisition.**Luciana S. Oliveira:**Investigation, Resources. **Valeria G. Alvarenga:**Investigation, Formal analysis.**Félix A. Urra:**Methodology, Investigation, Visualization, Writing - review & editing, Resources.**Jorge Toledo:**Methodology, Investigation, Formal analysis. **Armando Yarlequé:**Methodology, Resources, Supervision, Funding acquisition.**Johannes A. Eble:**Writing - review & editing, Funding acquisition.**Eladio F. Sanchez:**Resources, Methodology, Supervision, Project administration, Writing - review & editing, Funding acquisition.

## Acknowledgements

We thank S. Gontijo for her technical assistance. This work was supported by Convenio de Cooperación Bilateral CONCYTEC (Perú) – CNPq (Brazil), Grant 490269/2013-3, Fundação de Amparo y Pesquisa do Estado de Minas Gerais (FAPEMIG, Brazil, Grants APQ-01858-15, AUC-00022-16), Programa de Pos Graduação in Toxinology, Instituto Butantan, SP. Programa Nacional de Innovación para la Competitividad y Productividad – Innóvate Perú (Contrato N° 131- FINCyT-2013), Vicerrectorado de Investigación y Posgrado – Universidad Nacional Mayor de San Marcos, Perú (Proyectos N° B19101621, B17101271) and partially supported by FONDECYT-Chile postdoctoral fellowship #3170813, CONICYT-Chile PCI-Biotechnology #Redbio0027, FONDECYT-Chile: 1181823, ICM P09-015-F, EQM140038 and EQM140156. This report is part of a PhD Thesis of Dan Vivas-Ruiz, Post Graduate School in Biological Sciences, UNMSM. E.F.S, is Research Member of CNPq. J.A.E. received financial support for the German-Brazilian cooperation with E.F.S. from Deutsche Forschungsgemeinschaft (DFG-grant Eb177/13-1).

## Declaration of competing interest

The authors declared there is no conflict of interest.

## References

[1] K. Stocker, Medical Use of Snake Venoms Protein, CRC Press, Boca Raton, FL. Florida, 1990.
[2] F.S. Markland, Snake venoms and the hemostatic system, Toxicon 36 (1998) 1749–1800, https://doi.org/10.1016/S0041-0101(98)00126-3.
[3] S. Braud, C. Bon, A. Wisner, Snake venom proteins acting on hemostasis, Biochimie 82 (2000) 851–859, https://doi.org/10.1016/S0300-9084(00)01178-0.
[4] T. Sajevic, A. Leonardi, I. Krizaj, Hemostatically active proteins in snake venoms, Toxicon 57 (2011) 627–645, https://doi.org/10.1016/j.toxicon.2011.01.006.
[5] S. Serrano, The long road of research on snake venom serine proteinases, Toxicon 62 (2013) 19–26, https://doi.org/10.1016/j.toxicon.2012.09.003.
[6] M.J. Page, E. Di Cera, Serine peptidases: classification, structure and function, Cell. Mol. Life Sci. 65 (2008) 1220–1236, https://doi.org/10.1007/s00018-008-7565-9.
[7] S.M. Serrano, R.C. Maroun, Snake venom serine proteinases: sequence homology vs. substrate specificity, a paradox to be solved, Toxicon 45 (2005) 1115–1132, https://doi.org/10.1016/j.toxicon.2005.02.020.
[8] S. Braud, M.A. Parry, R. Maroun, C. Bon, A. Wisner, The contribution of residues 192 and 193 to the specificity of snake venom serine proteinases, J. Biol. Chem. 275 (2000) 1823–1828, https://doi.org/10.1074/jbc.275.3.1823.
[9] H.C. Castro, R.B. Zingali, M.G. Albuquerque, M. Pujol-Luz, C.R. Rodrigues, Snake venom thrombin-like enzymes: from reptilase to now, Cell. Mol. Life Sci. 61 (2004) 843–856, https://doi.org/10.1007/s00018-003-3325-z.
[10] A. Ullah, R. Masood, I. Ali, K. Ullah, H. Ali, H. Akbar, C. Betzel, Thrombin-like enzymes from snake venom: structural characterization and mechanism of action, Int. J. Biol. Macromol. 114 (2018) 788–811, https://doi.org/10.1016/j.ijbiomac.2018.03.164.
[11] N.D. Rawlings, A.J. Barret, A. Bateman, MEROPS: the database of proteolytic enzymes, their substrate and inhibitors, Nucleic Acids Res. 40 (2012) D343–D350.
[12] B. Oulion, J.S. Dobson, C.N. Zdenek, K. Arbuckle, C. Lister, F.C.P. Coimbra, B. Op den Brouw, J. Debono, A. Rogalski, A. Violette, R. Fourmy, N. Frank, B.G. Fry, Factor X activating Atractaspis snake venoms and the relative coagulotoxicity neutralizing efficacy of African antivenoms, Toxicol. Lett. 288 (2018) 119–128, https://doi.org/10.1016/j.toxlet.2018.02.020.
[13] K.W. Denson, F.E. Russell, D. Almagro, R.C. Bishop, Characterization of the coagulant activity of some snake venoms, Toxicon 10 (1972) 557–562.
[14] C. Yamamoto, D. Tsuru, N. Oda-Ueda, M. Ohno, S. Hattori, S.T. Kim, Flavoxobin, a serine protease from *Trimeresurus flavoviridis* (habu snake) venom, independently cleaves Arg726-Ser727 of human C3 and acts as a novel, heterologous C3 convertase, Immunology 107 (2002) 111–117, https://doi.org/10.1046/j.1365-2567.2002.01490.x.
[15] O. Costa Jde, K.C. Fonseca, C.C. Mamede, M.E. Beletti, N.A. Santos-Filho, A.M. Soares, E.C. Arantes, S.N. Hirayama, H.S. Selistre-de-Araújo, F. Fonseca, F. Henrique-Silva, N. Penha-Silva, F. de Oliveira, Bhalternin: functional and structural characterization of a new thrombin-like enzyme from *Bothrops alternatus* snake venom, Toxicon 55 (2010) 1365–1377, https://doi.org/10.1016/j.toxicon.2010.02.014.
[16] A. Magalhães, H.P.B. Magalhães, M. Richardson, S. Gontijo, R.N. Ferreira, A.P. Almeida, E.F. Sanchez, Purification and properties of a coagulant thrombin-like enzyme from the venom of *Bothrops leucurus*, Comp. Biochem. Physiol. A 146 (2007) 565–575, https://doi.org/10.1016/j.cbpa.2005.12.033.
[17] J.A. Campbell, W.W. Lamar, The Venomous Reptiles of the Western Hemisphere, Comstock, Publishing Associates, Ithaca, NY, 2004.
[18] C. Maguiña, C. Enrique, L. Ilquimiche, R. Mostorino, E. Gotuzzo, P. Legua, Ofidismo por *Bothrops pictus* en el Hospital Nacional Cayetano Heredia: Estudio prospectivo de 23 casos, Folia Dermatol. Perú. 9 (1998) 41–48.
[19] M. Kohlhoff, M.H. Borges, A. Yarleque, C. Cabezas, M. Richardson, E.F. Sanchez, Exploring the proteomes of the venoms of the Peruvian pit vipers *Bothrops atrox*, *B. barnetti* and *B. pictus*, J. Proteome 75 (2012) 2181–2195, https://doi.org/10.1016/j.jprot.2012.01.020.
[20] F. Lazo, D.E. Vivas-Ruiz, G.A. Sandoval, E.F. Rodríguez, E.E. Kozlova, F. Costal-Oliveira, C. Chávez-Olórtegui, R. Severino, A. Yarlequé, E.F. Sanchez EF, Biochemical, biological and molecular characterization of an L-amino acid oxidase (LAAO) purified from *Bothrops pictus* Peruvian snake venom, Toxicon 139 (2017) 74–86, https://doi.org/10.1016/j.toxicon.2017.10.001.
[21] D. Vivas-Ruiz, G.A. Sandoval, F. Lazo, E. Rodríguez, A. Yarlequé, E. Flores-Sánchez, Characterization of thrombin like enzyme from *Bothrops pictus* venom, Rev. Peru. Med. Exp. Salud Publica 32 (2015) 652–658, https://doi.org/10.17843/rpmesp.2015.324.1754.

[22] U.K. Laemmli, Cleavage of structural proteins during the assembly of the head of bacteriophage T4, Nature 227 (1970) 680–685.

[23] G.B. Naumann, L.F. Silva, L. Silva, G. Faria, M. Richardson, K. Evangelista, M. Kohlhoff, C.M. Gontijo, A. Navdaev, F.F. de Rezende, J.A. Eble, E.F. Sanchez, Cytotoxicity and inhibition of platelet aggregation caused by an L-amino acid oxidase from *Bothrops leucurus* venom, Biochim. Biophys. Acta 1810 (2011) 683–694, https://doi.org/10.1016/j.bbagen.2011.04.003.

[24] F.P. Silva-Junior, H.L. Guedes, L.C. Garvey, A.S. Aguiar, S.C. Bourguignon, E. Di Cera, S. Giovanni-De-Simone, BJ-48, a novel thrombin-like enzyme from the *Bothrops jararacussu* venom with high selectivity for Arg over Lys in P1: role of N-glycosylation in thermostability and active site accessibility, Toxicon 50 (2007) 18–31, https://doi.org/10.1016/j.toxicon.2007.02.018.

[25] D.E. Vivas-Ruiz, G.A. Sandoval, J. Mendoza, R.R. Inga, S. Gontijo, M. Richardson, J.A. Eble, A. Yarleque, E.F. Sanchez, Coagulant thrombin-like enzyme (barnettobin) from *Bothrops barnetti* venom: molecular sequence analysis of its cDNA and biochemical properties, Biochimie 95 (2013) 1476–1486, https://doi.org/10.1016/j.biochi.2013.03.015.

[26] A. Magalhães, H.P. Magalhães, M. Richardson, S. Gontijo, R.N. Ferreira, A.P. Almeida, E.F. Sanchez, Purification and properties of a coagulant thrombin-like enzyme from the venom of *Bothrops leucurus*, Comp. Biochem. Physiol. A Mol. Integr. Physiol. 146 (2007) 565–575, https://doi.org/10.1016/j.cbpa.2005.12.033.

[27] M.I. Estêvão-Costa, C.R. Diniz, A. Magalhães, F.S. Markland, E.F. Sanchez, Action of metalloproteinases mutalysin I and II on several components of the hemostatic and fibrinolytic systems, Thromb. Res. 99 (2000) 363–376, https://doi.org/10.1016/s0049-3848(00)00259-0.

[28] J. Konings, J.W. Govers-Riemslag, H. Philippou, N.J. Mutch, J.I. Borissoff, P. Allan, S. Mohan, G. Tans, H. Ten Cate, R.A. Ariëns, Factor XIIa regulates the structure of the fibrin clot independently of thrombin generation through direct interaction with fibrin, Blood 118 (2011) 3942–3951, https://doi.org/10.1182/blood-2011-03-339572.

[29] K. Laki, L. Lorandi, On the solubility of fibrin clots, Science 108 (1948) 280.

[30] R.D. Theakston, H.A. Reid, Development of simple standard assay procedures for the characterization of snake venom, Bull. World Health Organ. 61 (1983) 949–956.

[31] H. Kondo, S. Kondo, H. Ikezawa, R. Murata, Studies on the quantitative method for determination of hemorrhagic activity of Habu snake venom, Jpn. J. Med. Sci. Biol. 13 (1960) 43–52.

[32] M.I. Estevao-Costa, S.S. Gontijo, B.L. Correia, A. Yarleque, D. Vivas-Ruiz, E. Rodrigues, C. Chávez-Olortegui, L.S. Oliveira, E.F. Sanchez, Neutralization of toxicological activities of medically-relevant Bothrops snake venoms and relevant toxins by two polyvalent bothropic antivenoms produced in Peru and Brazil, Toxicon 122 (2016) 67–77, https://doi.org/10.1016/j.toxicon.2016.09.010.

[33] F.A. Urra, F. Muñoz, M. Córdova-Delgado, M.P. Ramírez, B. Peña-Ahumada B, M. Rios, P. Cruz, U. Ahumada-Castro, G. Bustos, E. Silva-Pavez, R. Pulgar, D. Morales D, D. Varela, J.P. Millas-Vargas, E. Retamal, O. Ramírez-Rodríguez, H. Pessoa-Mahana H, M. Pavani, J. Ferreira, C. Cárdenas, R. Araya-Maturana, FR58P1a; a new uncoupler of OXPHOS that inhibits migration in triple-negative breast cancer cells via Sirt1/AMPK/β1-integrin pathway, Sci. Rep. 4 (2018) 13190, https://doi.org/10.1038/s41598-018-31367-9.

[34] J. Schindelin, I. Arganda-Carreras, E. Frise, V. Kaynig, M. Longair, T. Pietzsch, S. Preibisch, C. Rueden, S. Saalfeld, B. Schmid, J.Y. Tinevez, D.J. White, V. Hartenstein, K. Eliceiri, P. Tomancak, A. Cardona, Fiji: an open-source platform for biological-image analysis, Nat. Methods 9 (2012) 676–682, https://doi.org/10.1038/nmeth.2019.

[35] A.J. Valente, L.A. Maddalena, E.L. Robb, F. Moradi, J.A. Stuart, A simple ImageJ macro tool for analyzing mitochondrial network morphology in mammalian cell culture, Acta Histochem. 119 (2017) 315–326, https://doi.org/10.1016/j.acthis.2017.03.001.

[36] F.A. Urra, M. Córdova-Delgado, M. Lapier, A. Orellana-Manzano, L. Acevedo-Arévalo, H. Pessoa-Mahana, J.M. González-Vivanco, M. Martínez-Cifuentes, O. Ramírez-Rodríguez, Small structural changes on a hydroquinone scaffold determine the complex I inhibition or uncoupling of tumoral oxidative phosphorylation, Toxicol. Appl. Pharmacol. 291 (2016) 46–57, https://doi.org/10.1016/j.taap.2015.12.005(J.P Millas-Vargas, B. Weiss-López, M. Pavani, J. Ferreira, R. Araya-Maturana).

[37] J.D. Thompson, T.J. Gibson, F. Plewniak, F. Jeanmougin, D.G. Higgins, The CLUSTAL_X windows interface: flexible strategies for multiple sequence alignment aided by quality analysis tools, Nucleic Acids Res. 25 (1997) 4876–4882, https://doi.org/10.1093/nar/25.24.4876.

[38] A. Sali, T.L. Blundell, Comparative protein modelling by satisfaction of spatial restraints, J. Mol. Biol. 234 (1993) 779–815, https://doi.org/10.1006/jmbi.1993.1626.

[39] A. Fiser, A. Sali, Modeller: generation and refinement of homology based protein structure models, Methods Enzymol. 374 (2003) 461–491, https://doi.org/10.1016/S0076-6879(03)74020-8.

[40] D. Eisenberg, R. Luthy, J.U. Bowie, VERIFY3D: assessment of protein models with three-dimensional profiles, Methods Enzymol. 277 (1997) 396–404, https://doi.org/10.1016/s0076-6879(97)77022-8.

[41] M. Wiederstein, M.J. Sippl, ProSA-web: interactive web service for the recognition of errors in three-dimensional structures of proteins, Nucleic Acids Res. 35 (2007) 407–410, https://doi.org/10.1093/nar/gkm290.

[42] C. Colovos, T.O. Yeates, Verification of protein structures: patterns of nonbonded atomic interactions, Protein Sci. 2 (1993) 1511–1519, https://doi.org/10.1002/pro.5560020916.

[43] R. Laskowski, M. Mac Arthur, D. Moss, J. Thornton, PROCHECK: a program to check the stereochemical quality of protein structures, J. Appl. Crystallogr. 26 (1993) 283–291, https://doi.org/10.1107/S0021889892009944.

[44] W.S. Delano, The PyMOL Molecular Graphics System, De lano Scientific, San Carlos, CA, 2002. http://www.pymol.org.

[45] S. Srinivasan, M. Guha, A. Kashina, N.G. Avadhani, Mitochondrial dysfunction and mitochondrial dynamics-the cancer connection, Biochim. Biophys. Acta Bioenerg. 1858 (2017) 602–614, https://doi.org/10.1016/j.bbabio.2017.01.004.

[46] M. Deshimaru, T. Ogawa, K.I. Nakashima, I. Nobuhisa, T. Chijiwa, Y. Shimohigashi, Y. Fukumaki, M. Niwa, I. Yamashina, S. Hattori, M. Ohno, Accelerated evolution of crotalinae snake venom gland serine proteases, FEBS Lett. 397 (1996) 83–88, https://doi.org/10.1016/s0014-5793(96)01144-1.

[47] R. Doley, S.P. Mackessy, R.M. Kini, Role of accelerated segment switch in exons to alter targeting (ASSET) in the molecular evolution of snake venom proteins, BMC Evol. Biol. 9 (2009) 146, https://doi.org/10.1186/1471-2148-9-146.

[48] A.F. Paes Leme, B.C. Prezoto, E.T. Yamashiro, L. Bertholim, A.K. Tashima, C.F. Klitzke, A.C. Camargo, S.M. Serrano, Bothrops protease A, a unique highly glycosylated serine proteinase, is a potent, specific fibrinogenolytic agent, J. Thromb. Haemost. 6 (2008) 1363–1372, https://doi.org/10.1111/j.1538-7836.2008.02995.x.

[49] F.L. Costa, R.S. Rodrigues, L.F. Izidoro, D.L. Menaldo, A. Hamaguchi, M.I. Homsi-Brandeburgo, A.L. Fuly, S.G. Soares, H.S. Selistre-de-Araújo, B. Barraviera, A.M. Soares, V.M. Rodrigues, Biochemical and functional properties of a thrombin-like enzyme isolated from *Bothrops pauloensis* snake venom, Toxicon 54 (2009) 725–735, https://doi.org/10.1016/j.toxicon.2009.05.040.

[50] D.J. Phillips, S.D. Swenson, F.S. Markland, Thrombin-like snake venom serine proteinases, in: S.P. Mackessy (Ed.), Handbook of Venoms and Toxins of Reptiles, CRC Press, New York, London 2010, pp. 139–152.

[51] N.A. Marsh, Snake venoms affecting the haemostatic mechanism a consideration of their mechanisms, practical applications and biological significance, Blood Coagul. Fibrinolysis 5 (1994) 399–410.

[52] N. Marsh, V. Williams, Practical applications of snake venom toxins in haemostasis, Toxicon 45 (2005) 1171–1181, https://doi.org/10.1016/j. toxicon.2005.02.016.

[53] D.E. Levy, G.J. Del Zoppo, Ancrod: a potential treatment for acute ischemic stroke from snake venom, Toxicol. Rev. 25 (2006) 323–333, https://doi.org/10.1080/15569540600567354.

[54] B. Blombäck, B. Hessel, D. Hogg, L. Therkildsen, A two-step fibrinogen-fibrin transition in blood coagulation, Nature 275 (1978) 501–505, https://doi.org/10.1038/275501a0.

[55] C.M. Teng, F.N. Ko, Comparison of the platelet aggregation induced by three thrombin-like enzyme of snake venoms and thrombin, Thromb. Haemost. 59 (1988) 304–309.

[56] S. Niewiarowski, E.P. Kirby, T.M. Brudzynski, K. Stocker, Thrombocytin, a serine protease from *Bothrops atrox* venom. 2. Interaction with platelets and plasma-clotting factors, Biochemistry 18 (1979) 3570–3577, https://doi.org/10.1021/bi00583a021.

[57] S.M. Serrano, R. Mentele, C.A. Sampaio, E. Fink, Purification, characterization, and amino acid sequence of a serine proteinase, PA-BJ, with platelet-aggregating activity from the venom of *Bothrops jararaca*, Biochemistry 34 (1995) 7186–7193, https://doi.org/10.1021/bi00021a033.

[58] K.F. Stocker, J. Meier, Thrombin- like snake venom enzymes, in: H. Pirkle, F.S. Markland (Eds.), Hemostasis and Animal Venoms, Vol. 7, Marcel Dekker Inc., New York 1988, pp. 67–84.

[59] L. Polgár, The catalytic triad of serine peptidases, Cell. Mol. Life Sci. 62 (2005) 2161–2172, https://doi.org/10.1007/s00018-005-5160-x.

[60] A.J. Barrett, P.M. Starkey, The interaction of alpha α2-macroglobulin with proteinases, characteristics and specificity of the reaction and hypothesis concerning its molecular mechanism, Biochem. J. 133 (1973) 709–724, https://doi.org/10.1042/bj1330709.

[61] S.R. Feldman, L.S. Gonias, S.V. Pizzo, Model of α2-macroglobulin structure and function, Proc. Natl. Acad. Sci. U. S. A. 82 (1985) 5700–5704, https://doi.org/10.1073/pnas.82.17.5700.

[62] A. Magalhães, R. Ferreira, M. Richardson, S. Gontijo, A. Yarleque, H. Magalhaes, C. Bloch, E. Sanchez, Coagulant thrombin-like enzymes from the venoms of Brazilian and Peruvian bushmaster (*Lachesis muta muta*) snakes, Comp. Biochem. Physiol. B 136 (2003) 255–266, https://doi.org/10.1016/S1096-4959(03)00202-1.

[63] J.P. Steiner, P. Bhattacharya, D.K. Strickland, Thrombin- induced conformational changes of human α2-macroglobulin: evidence for two functional domains, Biochemistry 24 (1985) 2993–3001, https://doi.org/10.1021/bi00333a028.

[64] J. Huntington, Molecular recognition mechanisms of thrombin, J. Thromb. Haemost. 3 (2005) 1861–1872, https://doi.org/10.1111/j.1538-7836.2005.01363.x.

[65] S. Braud, B.F. Le Bonniec, C. Bon, A. Wisner, The stratagem utilized by the plasminogen activator from the snake *Trimeresurus stejnegeri* to escape serpins, Biochemistry 41 (2002) 8478–8484, https://doi.org/10.1021/bi016069g.

[66] D. Hanahan, R.A. Weinberg, Hallmarks of cancer: the next generation, Cell 144 (2011) 646–674, https://doi.org/10.1016/j.cell.2011.02.013.

[67] F.A. Urra, B. Weiss-Lopez, R. Araya-Maturana, Determinants of anti-cancer effect of mitochondrial electron transport chain inhibitors: bioenergetic profile and metabolic flexibility of cancer cells, Curr. Pharm. Des. 22 (2016) 5998–6008, https://doi.org/10.2174/1381612822666160719122626.

[68] F.A. Urra, F. Munoz, A. Lovy, C. Cardenas, The mitochondrial complex(I)ty of cancer, Front. Oncol. 7 (2017) 118, https://doi.org/10.3389/fonc.2017.00118.

[69] V.S. LeBleu, J.T. O'Connell, K.N. Gonzalez Herrera, H. Wikman, K. Pantel, M.C. Haigis, F.M. de Carvalho, A. Damascena, L.T. Domingos Chinen, R.M. Rocha, J.M. Asara, R. Kalluri, PGC-1α mediates mitochondrial biogenesis and oxidative phosphorylation in cancer cells to promote metastasis, Nat. Cell Biol. 16 (2014) 992–1003, https://doi.org/10.1038/ncb3039.

[70] S. Andrzejewski, E. Klimcakova, R.M. Johnson, S. Tabariès, M.G. Annis, S. McGuirk, J.J. Northey, V. Chénard, U. Sriram, D.J. Papadopoli, P.M. Siegel, J. St-Pierre, PGC-1α promotes breast Cancer metastasis and confers bioenergetic flexibility against metabolic drugs, Cell Metab. 26 (2017) 778–787, https://doi.org/10.1016/j.cmet.2017.09.006.

[71] U. Logonder, Z. Jenko-Praznikar, T. Scott-Davey, J. Pungercar, I. Krizaj, J.B. Harris, Ultrastructural evidence for the uptake of a neurotoxic snake venom phospholipase A2 into mammalian motor nerve terminals, Exp. Neurol. 219 (2009) 591–594, https://doi.org/10.1016/j.expneurol.2009.07.017.

[72] M.L. Massimino, M. Simonato, B. Spolaore, C. Franchin, G. Arrigoni, O. Marin, L. Monturiol-Gross, J. Fernández, B. Lomonte, F. Tonello, Cell surface nucleolin interacts with and internalizes *Bothrops asper* Lys49 phospholipase A2 and mediates its toxic activity, Sci. Rep. 8 (2018), 10619. https://doi.org/10.1038/s41598-018-28846-4.

[73] B. Zhang, F. Li, Z. Chen, I.H. Shrivastava, E.S. Gasanoff, R.K. Dagda, *Naja mossambica mossambica* cobra cardiotoxin targets mitochondria to disrupt mitochondrial membrane structure and function, Toxins (Basel) 11 (2019) https://doi.org/10.3390/toxins11030152pii: E152.

[74] N. Corona de la Peña, M. Gutiérrez-Aguilar, I. Hernández-Reséndiz, A. Marín-Hernández, S. Rodríguez-Enríquez, Glycoprotein Ib activation by thrombin stimulates the energy metabolism in human platelets, PLoS One 12 (2017) e0182374, https://doi.org/10.1371/journal.pone.0182374Aug 17.